INVESTIGATING CATALYTIC SELECTIVITY OF NANOPARTICLES ENCAPSULATED IN MOFS

Chenhao Ren

A thesis
submitted to the Faculty of
the department of Chemistry
in partial fulfillment
of the requirements for the degree of
Master of Science

Boston College
Morrissey College of Arts and Sciences
Graduate School

2021 April

INVESTIGATING CATALYTIC SELECTIVITY OF NANOPARTICLES ENCAPSULATED IN MOFS

Chenhao Ren

Advisor: Prof. Chia-Kuang Tsung

Abstract

Coating porous materials is a potential pathway to improve Catalytic performance of heterogeneous catalysts. The unique properties of Metal organic frameworks (MOFs) like huge surface area, long range order and high tenability make them promising coating materials. However, two traditional MOF encapsulation methods have their own issues. Herein, we synthesized Pt/Pd metal nanoparticles @UiO-66-NH$_2$ via a one-pot *in situ* method which has good control of nanoparticles size while avoids the introduction of capping agent. The catalytic performance of synthesized Pt@UiO-66-NH$_2$ is tested via selective hydrogenation of Crotonaldehyde. And the selectivity of our desired product achieves 70.42% which is much higher than merchant Pt catalysts. A step further, we used linker exchange to replace the original NH$_2$-BDC linker of which amine group plays an important role in the coating process. After linker exchanging, the significant decreasing in selectivity of our target product demonstrates that the interaction between Pt and amine group does have some positive impacts on their catalytic performance. We hope our research could provide some insights of the MOFs and nanoparticles interface

and help rational design of catalysts with high performance.

Table of Contents

Acknowledgements

List of Abbreviations

MOF	Metal Organic Frameworks
UiO-66	Universitet i Oslo (a kind of MOF)
PVP	Polyvinyl Pyrrolidone
CTAB	Cetyltrimethylammonium Bromide
SEM	Scanning Electronic Microscope
TEM	Transmission Electronic Microscope
NMR	Nuclear Magnetic Resonance
XRD	X-ray powder diffraction
GC-MS	Gas chromatography–mass spectrometry
ICP-OES	Inductively Coupled Plasma-Optical Emission Spectrometry
BDC	terephthalic acid/1,4-Benzenedioic acid

List of Figures

List of Tables

.

Chapter 1 Introduction

1.1 Metal Nanoparticles as Catalysts

Nanomaterials are materials of which at least one dimension of a single unit is in nanoscales (usually defined as 1-100 nm). Differing from separated molecules/atoms or bulk materials, nanomaterials have unique optical, electronic, or mechanical properties due to high surface to volume ratio and high surface energy. Basically, nanoparticles are usually synthesized by three kinds of techniques: i) vapor condensation, ii) colloidal chemical reaction and iii) solid state processes. In recent 30 years, preparations and applications of different nanomaterials have been widely and rapidly developed by numerous talented scientists. Nowadays, not only pure nanomaterials but hybrid[1, 2] or complicated-structured ones can be controlled or half-controlled synthesized and are widely used in industry and our daily life, which are expected to play more and more important roles in solving some major issues of human society like energy shortage and environmental protection. Due to these unique properties, performing as catalysts is one of the greatest applications of nanoparticles.

Catalysts can be divided into two categories, homogeneous and heterogeneous catalysts, depending on whether they occupy the same phase as the reaction mixture or not. Homogeneous catalysts which stay in the same phase with the reaction mixture are usually small organic/inorganic molecules or organometallic complexes. The relatively simple structures mean the precise control of synthesis process of homogeneous catalysts is technically accessible, which leads to well-defined active sites and higher selectivity

for certain reactions. Typically, organometallic complexes, as a widely used series of homogeneous catalysts, can be synthesized with rational design to achieve very high activity and selectivity for a target reaction. An experienced and skillful chemist can optimism the electronic and steric properties of an organometallic complex by simply altering the central transition metal and/or coordinated ligands, which can lead to predictable changes in activity and/or selectivity. Meanwhile, the efficient and powerful characterization methods for homogenous catalysts such as NMR spectroscopy and IR spectroscopy further predigest the problem.

Heterogeneous catalysts have better potential for large-scale industry applications because they can be separated from reaction mixture and reused by easier ways, like filtration, due to the phase difference. Usually, heterogeneous catalysts are solids which means higher thermal and chemical stability comparing to homogenous catalysts. However, unlike the uniform active sites for homogeneous catalysts, the active sites which are usually defects on the catalysts surface are much more complicated and still lacking of control during the synthesis process, which leads to poor selectivity. Meanwhile, the phase difference in a heterogeneous catalytic reaction makes it much more complicated. Reaction can only occur in the interface of homogeneous catalysts and reaction mixture (gas or solution), so catalysts are loaded onto porous support materials and/or synthesized in nano scale to improve the surface to volume ratio to achieve higher activity. But the support materials will also influence the chemical and steric environments of the active sites, making the precise control of selectivity even harder. And for nanoparticle catalysts, a huge problem comes from the capping agents which are

widely used to tune the crystallization process to achieve desired geometry and stabilize the sub stable particles. These capping agents (usually surfactants) bind tightly on the nanoparticle surface and block active sites, causing the magnificent loss of catalytic activity and selectivity control.

Based on the advantages and shortcomings of homogenous and heterogeneous catalysts, Great efforts are made by scientists to set up new strategies to take advantages of both kinds of catalysts, like fixing classical homogenous catalysts on supporting materials or making "single-atom" catalysts. [3-7]. Among those strategies, coating nanoparticle heterogeneous catalysts with porous materials is a promising solution to the poor control of the electronic and steric environments around active sites on heterogeneous catalysts. By modifying the chemical components or topological of the porous material, at the interface, the chemical environment around active sites can also be changed. Also, by replacing the absorbed capping agents on the nanoparticle surface, porous materials can act as stabilizer and improve its activity. In order to achieve this, we need to have a better understanding of what really happens in the interface of nanoparticles and coating materials as the electronic and spatial environments near the active sites is the key to get high activity and selectivity. Thus, metal organic frameworks (MOFs), as crystalline porous materials with fully tunable topological and chemical pore environments, were chosen to form metal nanoparticles@porous materials core-shell structure. It has been repeatedly reported that taking use of the tunability of MOFs to optimize the catalytic performance of metal nanoparticles@MOFs core-shell structure.[8, 9]

1.2 Metal Organic Frameworks

Metal Organic Frameworks (MOFs) are a kind of organic-inorganic hybrid crystalline materials made up of metal-containing secondary building units (SBUs, usually metal notes or clusters) and organic linkers. These two parts are connected by coordination bonds and form a long-rang ordered crystalline structure with accessible channels. (Figure **1.1**) In the recent 20 years, MOFs have drawn lots of attentions due to their high surface area, uniform pores and tunable chemical compositions [10]which demonstrate the tremendous potential applications of MOFs for gas separation and storage, catalysis, drug delivery and many other fields.[11]

Metal ions or clusters   **Organic linkers**   **Metal-organic framework**
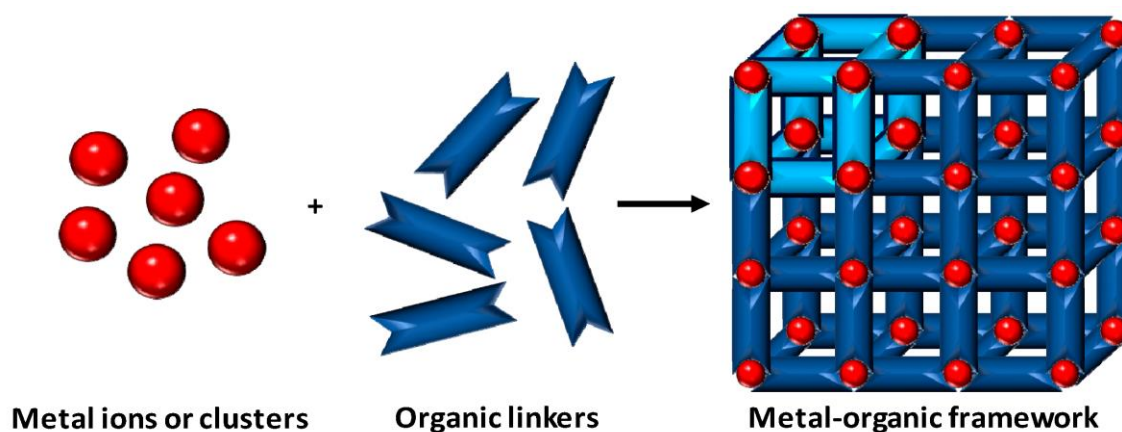
Figure 1.1 Scheme of typical preparation of MOFs. Combination of metal ions or clusters with organic linkers to form a cross-linked network.[12]

SBUs and organic linkers in MOFs have many possible combinations, which leads to more than 20,000 found MOFs and the number is keeping increasing every day. (**Figure 1.2**) The incredible tunability of building blocks gives MOFs great tunability. The coordination interaction between SBUs and organic linkers determines the topologies of the formed MOFs which alters with the nature of two parts and synthesis conditions. By

optimizing the chain length of the organic linker, different pore sizes can be easily achieved. Also, the functional groups on the side chain of organic linkers provides countless possibilities for MOFs. Also, unlike some zeolites or polymers which are not convenient to modify after solidify, MOFs can be also postsynthetic modified (PSM) by various pathways, like ligand incorporation, atomic layer deposition and linker exchange, which further expand their possible application range.[13, 14]
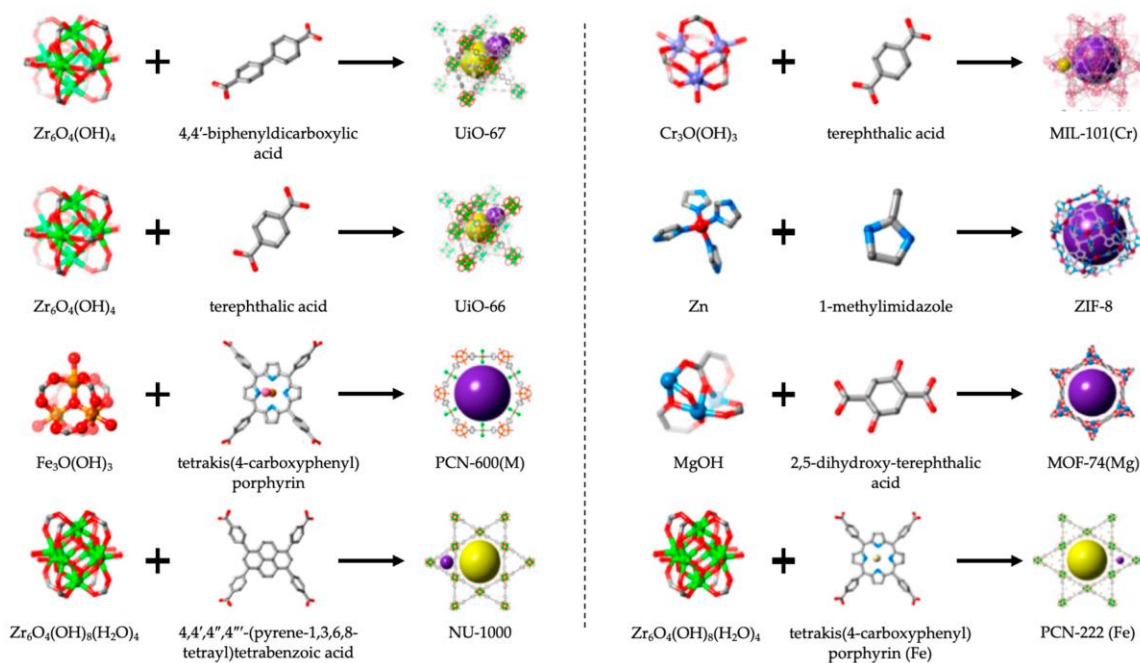
Figure 1.2 Some typical MOFs with different SBUs and organic linkers.[15]

However, the organic-inorganic hybrid nature of MOFs also results in some drawbacks. Comparing to pure inorganic materials like zeolite, MOFs usually can't resist high temperature. And many MOFs will undergo hydrolysis process in strong/weak acidic/basic solutions due to the feature of coordination bonds. Lacking of thermal and chemical stability restricts the actual application of MOFs. Luckily, robust MOFs with hyper thermal and chemical stability were developed and widely studied. One of the most

robust one is the Zirconium-based MOF, UiO-66. UiO-66 is made up of zirconium-oxo cluster nodes ($Zr_6O_4(OH)_4$ octahedra cluster) and terephthalic acid (also known as 1,4-Benzenedioic acid, BDC) linkers. Each SBU is connected to 12 BDC linkers, forming 3D network with octahedral and tetrahedral cages **(Figure 1.3)**. As expected, UiO-66 shows outstanding chemical and thermal stability because of the strong zirconium-oxygen bond. The MOF can maintain the structure under high temperature up to 500 °C and won't break down till 800 °C. UiO-66 resists all regular strong acids and bases and can only be digested by HF. Meanwhile, UiO-66 has an aperture size of 0.5nm which is close to the size of small organic compounds, making it a promising catalyst support. The benzene ring of the BDC linker can be functionalized with ease, providing further tunability. With these superior properties, UiO series MOFs and their derivatives shows potential for numerous applications, such as catalysis, gas absorption, waste water treatment. [16-18]
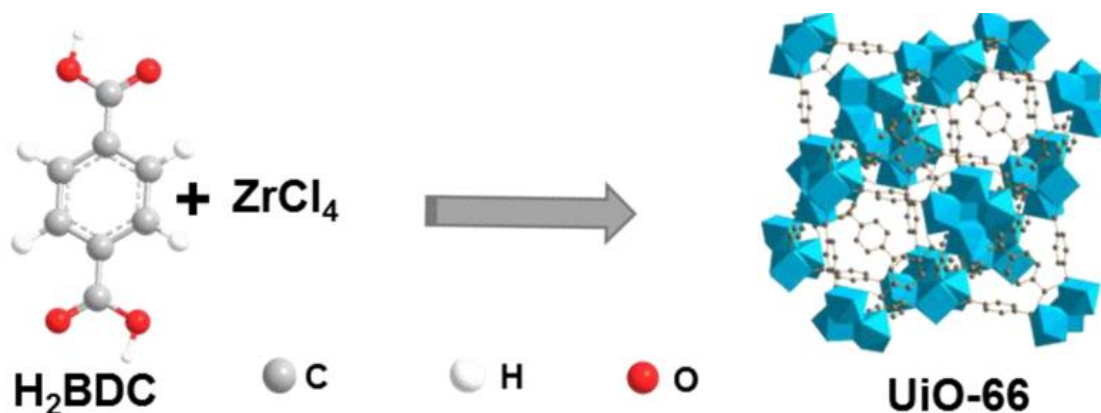
Figure 1.3 Structure of UiO-66[19]

1.3 Metal NPs@Metal Organic Frameworks Core-Shell Structure

1.3.1 Properties Resulted from MOFs as Coating Shell

Basically, NPs@MOFs core-shell structures can be divided into three types: one-to-one NP@MOF, multiple NPs@MOF and york-shell NP@hollow MOF (**Figure 1.4**). Different encapsulation forms have different properties and performance. The Tsung group have done some works about synthesis and properties of One-to-one NP@MOFs core-shell structures which have very uniform structures and good aliment between nanoparticles and MOFs, making them good samples for diffusion and mechanism studies. [9, 20]Metal nanoparticles' size in multiple NPs@MOF is usually restricted by pore size of the MOF which may lead to higher activity (because of high surface to volume ratio) but also means less control of the nanoparticles' size and distribution. [21-27]There are more room and less restriction for york-shell NP@MOF structure which is good for encapsulation of homogeneous catalysts. In this thesis, we mainly synthesized and studied one type of multiple NPs @MOF.
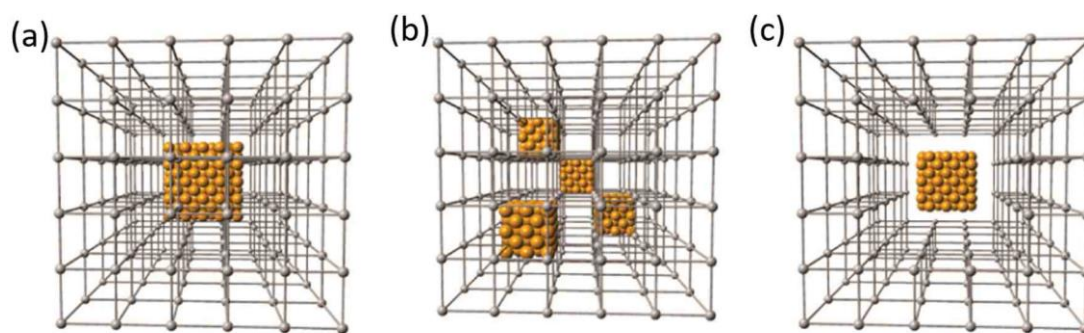
Figure 1.4 (a) One-to-one NP@MOF. (b) multiple NPs@MOF. (c) york-shell NP@hollow MOF. Reprinted with permission.[9] Copyright © 2014, American Chemical Society.

Nowadays, it is highly desired to develop a systematic method to provide well-controlled coordination environment around active sites for heterogeneous catalysts. Applying porous materials on the surface of metal nanoparticles is a promising solution for this. Basically, those porous materials shells around metal NPs can provide physical protection which prevents aggregation of those metal NPs to increase their stability. Also, some porous materials like MOFs have uniform porous structures and their pore size varies with different types of MOFs, which can be used to introduce size selectivity for heterogeneous catalysts.[25, 28] Comparing with other porous materials, firstly, MOFs are crystalline materials which means MOFs coating layers will provide more uniform influence to metal NPs cores which is more convenient for deeper digging of mechanism and further modification. [29]Secondly, MOFs have a huge family which has more than 20,000 members so that they can provide tons of different chemical/electronic and topological environments around metal NPs. Thirdly, since MOFs are made up of metal nodes and organic linkers via coordination interaction, they can be further modified even after synthesis.

1.3.2   Approaches to Synthesize Metal NPs@MOFs

Generally speaking, there are two widely used traditional strategies for encapsulating metal nanoparticles into metal organic frameworks. One is post impregnation approach (ship in bottle) and the one is *de novo* approach (bottle around ship).[30, 31]
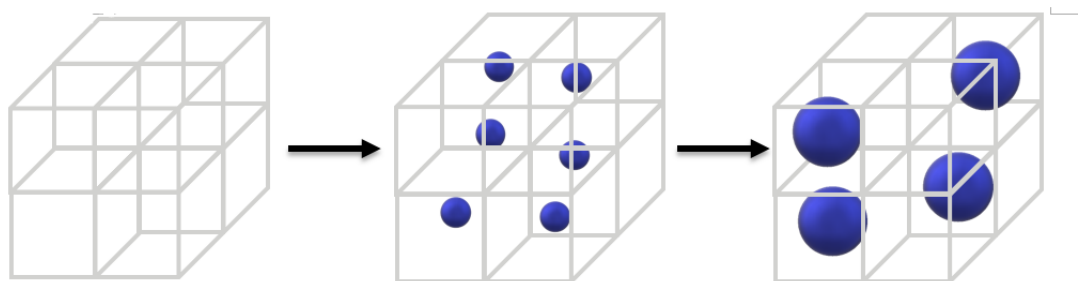
Pre-synthesized MOFs   Infiltration of metal precursors   Formation of metal NPs

Figure 1.5 Scheme of post impregnation approach (ship in bottle), small blue balls, huge blue balls and grey frameworks represent for nanoparticles precursors, nanoparticles and MOFs respectively

For the post impregnation (ship in bottle) method, metal organic frameworks will be synthesized firstly, then precursors of metal nanoparticles will be mixed together with pre-synthesized metal organic frameworks.[32-35] And those precursors will infiltrate into the pores and cavities of those MOFs via diffusion or assisted diffusion. Sometimes, some functional groups will be introduced to the backbones of MOFs to increase their interaction with the nanoparticle precursors. Then under certain conditions like reduction environment or calcination, those precursors will be transformed to metal nanoparticles. During the synthesis process, except for the size restriction due to the volume of the cages or pores, it is very likely to lose control of shape, size and amount of formed metal nanoparticles. Also, some metal NPs will form on the external surface of MOFs instead of inside. (**Figure 1.5**)

For the *de novo* approach (bottle around ship), metal nanoparticles will be synthesized at very beginning, and then be added into the synthetic environment of metal organic

frameworks. [20, 21, 36, 37]Then MOFs will grow around those metal nanoparticles and finally form encapsulation structures. (**Figure 1.6**) For this approach, we can get well-defined metal nanoparticles with decent shape and size control since nanoparticles are pre-synthesized. However, during the synthetic process of metal nanoparticles, capping agents such as PVP (polyvinyl pyrrolidone) or CTAB (Cetyltrimethylammonium bromide) are used to tune the growth of metal nanoparticles to achieve geometric control of them. And those capping agents are usually firmly bound to the surface of those nanoparticles and help to stabilize those active surfaces with high surface energy, which are hard to remove in washing and encapsulation process. As a result, those capping agents which usually bind to active sites of encapsulated nanoparticles will influence catalytic performance of those heterogeneous catalysts badly.
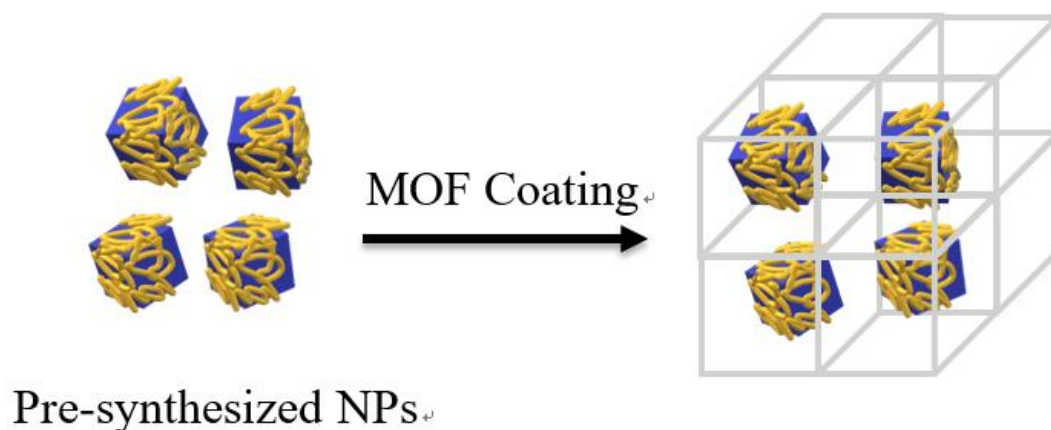
Figure 1.6 Scheme of *de novo* approach (bottle around ship), blue cubes, yellow lines and grey frameworks represent for nanoparticles, capping agents and MOFs respectively

Due to the major issues of these two traditional encapsulation methods, a new strategy called one pot approach has been developed recently.[38]Considering the interaction of MOF linkers with metal nanoparticles precursors and surfaces, it is possible for organic

linkers to replace the conventional capping agents. With this interaction, not only use of annoying capping agents can be avoided but the growth of metal nanoparticles can be better controlled. For one pot approach, nanoparticles precursors and metal organic framework precursors will be mixed together. Under certain reaction conditions, reduction of metal precursors and growth of MOFs on the surface of generated metal NPs will happen subsequently. (**Figure 1.7**) In order to achieve expected results, two critical problems of this method need to be solved: Well control of the interaction between MOFs linker and metal nanoparticles to ensure MOFs linkers play the role of capping agent to approve well- control of formed metal NPs, controlled formation of MOFs around generated metal NPs instead of homogeneous nucleation in solution. Because of the complexity of these reaction systems, only a part of metal NPs@MOFs can be synthesized by this method. However, for those limited types of NPs@MOFs synthesized by this method, we can hope to get well-defined metal NPs with controllable size, shape morphology and clean surface. In this thesis, we will study catalytic performance of a type of NPs@MOFs synthesized via one-pot approach.
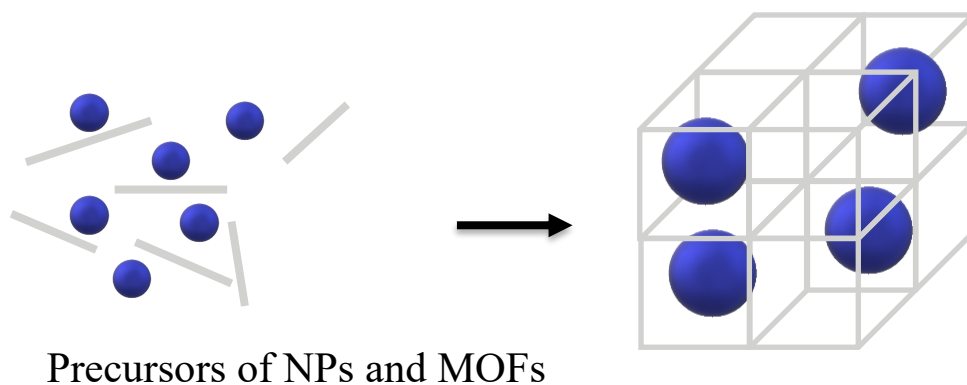
Precursors of NPs and MOFs

Figure 1.7 Scheme of one pot approach, small blue balls, huge blue balls, short grey lines and grey frameworks represent for nanoparticles precursors, nanoparticles, MOF precursors and MOFs respectively

1.4 Reference

1.   Hoener, C.F., et al., *Demonstration of a shell-core structure in layered cadmium selenide-zinc selenide small particles by x-ray photoelectron and Auger spectroscopies.* The Journal of Physical Chemistry, 1992. **96**(9): p. 3812-3817.

2.   Spanhel, L., H. Weller, and A. Henglein, *Photochemistry of semiconductor colloids. 22. Electron ejection from illuminated cadmium sulfide into attached titanium and zinc oxide particles.* Journal of the American Chemical Society, 1987. **109**(22): p. 6632-6635.

3.   Yang, X.-F., et al., *Single-Atom Catalysts: A New Frontier in Heterogeneous Catalysis.* Accounts of Chemical Research, 2013. **46**(8): p. 1740-1748.

4.   Wang, A., J. Li, and T. Zhang, *Heterogeneous single-atom catalysis.* Nature Reviews Chemistry, 2018. **2**(6): p. 65-81.

5.   Parkinson, G.S., *Single-Atom Catalysis: How Structure Influences Catalytic Performance.* Catalysis Letters, 2019. **149**(5): p. 1137-1146.

6.   Zhang, H., et al., *Single-Atom Catalysts: Emerging Multifunctional Materials in Heterogeneous Catalysis.* Advanced Energy Materials, 2018. **8**(1): p. 1701343.

7.   Liu, Q. and Z. Zhang, *Platinum single-atom catalysts: a comparative review towards effective characterization.* Catalysis Science & Technology, 2019. **9**(18): p. 4821-4834.

8.   Hendon, C.H., et al., *Grand Challenges and Future Opportunities for Metal–Organic Frameworks.* ACS Central Science, 2017. **3**(6): p. 554-563.

9.   Hu, P., J.V. Morabito, and C.-K. Tsung, *Core–Shell Catalysts of Metal Nanoparticle Core and Metal–Organic Framework Shell.* ACS Catalysis, 2014. **4**(12): p. 4409-4419.

10.   Lu, G. and J.T. Hupp, *Metal–Organic Frameworks as Sensors: A ZIF-8 Based Fabry–Pérot Device as a Selective Sensor for Chemical Vapors and Gases.* Journal of the American Chemical Society, 2010. **132**(23): p. 7832-7833.

11.   Lee, J., et al., *Metal–organic framework materials as catalysts.* Chemical Society Reviews, 2009. **38**(5): p. 1450-1459.

12.   Carrasco, S., *Metal-Organic Frameworks for the Development of Biosensors: A Current Overview.* Biosensors (Basel), 2018. **8**(4).

13.   Islamoglu, T., et al., *Postsynthetic Tuning of Metal–Organic Frameworks for Targeted Applications.* Accounts of Chemical Research, 2017. **50**(4): p. 805-813.

14.   Kreno, L.E., et al., *Metal–Organic Framework Materials as Chemical Sensors.* Chemical Reviews, 2012. **112**(2): p. 1105-1125.

15.   Gutiérrez, S., et al., *Metal–Organic Frameworks as Key Materials for Solid-Phase Microextraction Devices—A Review.* Separations, 2019. **6**(4).

16.   Cmarik, G.E., et al., *Tuning the Adsorption Properties of UiO-66 via Ligand Functionalization.* Langmuir, 2012. **28**(44): p. 15606-15613.

17.   Anjum, M.W., et al., *Modulated UiO-66-Based Mixed-Matrix Membranes for CO2 Separation.* ACS Applied Materials & Interfaces, 2015. **7**(45): p. 25193-25201.

18.   Dhakshinamoorthy, A., et al., *Engineering UiO-66 Metal Organic Framework for Heterogeneous Catalysis.* ChemCatChem, 2019. **11**(3): p. 899-923.

19.   Xu, W., et al., *A Facile Method for Preparing UiO-66 Encapsulated Ru Catalyst and its Application in Plasma-Assisted CO2 Methanation.* Nanomaterials, 2019. **9**(10): p. 1432.

20.   Hu, P., et al., *Surfactant-Directed Atomic to Mesoscale Alignment: Metal Nanocrystals Encased Individually in Single-Crystalline Porous Nanostructures.* Journal of the American Chemical Society, 2014. **136**(30): p. 10561-10564.

21.   Lu, G., et al., *Imparting functionality to a metal–organic framework material by controlled nanoparticle encapsulation.* Nature Chemistry, 2012. **4**(4): p. 310-316.

22.   Zhang, W., et al., *A Family of Metal-Organic Frameworks Exhibiting Size-Selective Catalysis with Encapsulated Noble-Metal Nanoparticles.* Advanced Materials, 2014. **26**(24): p. 4056-4060.

23.   Aijaz, A., et al., *Metal–Organic Framework-Immobilized Polyhedral Metal Nanocrystals: Reduction at Solid–Gas Interface, Metal Segregation, Core–Shell Structure, and High Catalytic Activity.* Journal of the American Chemical Society, 2013. **135**(44): p. 16356-16359.

24.   Esken, D., et al., *Au@ZIFs: Stabilization and Encapsulation of Cavity-Size Matching Gold Clusters inside Functionalized Zeolite Imidazolate Frameworks, ZIFs.* Chemistry of Materials, 2010. **22**(23): p. 6393-6401.

25.   Jiang, H.-L., et al., *Au@ZIF-8: CO Oxidation over Gold Nanoparticles Deposited to Metal–Organic Framework.* Journal of the American Chemical Society, 2009. **131**(32): p. 11302-11303.

26.   Sugikawa, K., et al., *Stable and Functional Gold Nanorod Composites with a Metal–Organic Framework Crystalline Shell.* Chemistry of Materials, 2013. **25**(13): p. 2565-2570.

27.   Tsuruoka, T., et al., *Controlled Self-Assembly of Metal–Organic Frameworks on Metal Nanoparticles for Efficient Synthesis of Hybrid Nanostructures.* ACS Applied Materials & Interfaces, 2011. **3**(10): p. 3788-3791.

28.   Kuo, C.-H., et al., *Yolk–Shell Nanocrystal@ZIF-8 Nanostructures for Gas-Phase Heterogeneous Catalysis with Selectivity Control.* Journal of the American Chemical Society, 2012. **134**(35): p. 14345-14348.

29.   Chen, L., R. Luque, and Y. Li, *Controllable design of tunable nanostructures inside metal–organic frameworks.* Chemical Society Reviews, 2017. **46**(15): p. 4614-4630.

30.   Falcaro, P., et al., *Application of metal and metal oxide nanoparticles@MOFs.* Coordination Chemistry Reviews, 2016. **307**: p. 237-254.

31.   Yu, J., et al., *Nanoparticle/MOF composites: preparations and applications.* Materials Horizons, 2017. **4**(4): p. 557-569.

32.   Rösler, C. and R.A. Fischer, *Metal–organic frameworks as hosts for nanoparticles.* CrystEngComm, 2015. **17**(2): p. 199-217.

33.   Zlotea, C., et al., *Pd Nanoparticles Embedded into a Metal-Organic Framework: Synthesis, Structural Characteristics, and Hydrogen Sorption Properties.* Journal of the American Chemical Society, 2010. **132**(9): p. 2991-2997.

34.   He, L., et al., *Silver nanoparticles prepared by gamma irradiation across metal–organic framework templates.* RSC Advances, 2015. **5**(14): p. 10707-10715.

35.   Houk, R.J.T., et al., *Silver Cluster Formation, Dynamics, and Chemistry in Metal–Organic Frameworks.* Nano Letters, 2009. **9**(10): p. 3413-3418.

36.   Doherty, C.M., et al., *Using Functional Nano- and Microparticles for the Preparation of Metal–Organic Framework Composites with Novel Properties.* Accounts of Chemical Research, 2014. **47**(2): p. 396-405.

37.   Zhang, K., et al., *Exploring the Framework Hydrophobicity and Flexibility of ZIF-8: From Biofuel Recovery to Hydrocarbon Separations.* The Journal of Physical Chemistry Letters, 2013. **4**(21): p. 3618-3622.

38.   Chen, L., et al., *One-step encapsulation of Pd nanoparticles in MOFs via a temperature control program.* Journal of Materials Chemistry A, 2015. **3**(29): p. 15259-15264.

Chapter 2 Synthesis and Characterization of Metal NPs@UiO-66-NH$_2$

2.1 Introduction

Thanks to Dr. Allison Young for her great contribution for this part of work.

As discussed in Chapter 1, encapsulating metal nanoparticles with MOFs has been considered as a promising approach to adjust their catalytic performance. Due to the drawbacks for two conventional encapsulation method, one-pot encapsulation strategy was developed to get nanoparticles inside with geometry control and clean surface.

Inspired by Yingwei Li' previous work[1], we successfully encapsulated Pt and Pd nanoparticles into UiO-66-NH$_2$ Via an One-pot method. As discussed in Chapter 1, UiO-66 was chosen as host material due to its high thermal and chemical stability.[2, 3] The introduction of amine group in the original linker is a key factor of the formation of the core-shell structure, during the synthesis process, the interaction between lone pair electrons of N in amine group and metal precursors will ensure the encapsulation. [4, 5]Pt and Pd are selected here due to their wide applications as catalysts. [6-15]In a typical synthesis procedure, Pd/Pt precursor, Zr precursor, BDC-NH$_2$ and reaction modulator acetic acid are dissolved in DMF which acts as both solvent and reducing agent. Then the reaction mixture was heated to a certain temperature for 24 hours for the core-shell structure to form. (**Figure 2.1**)
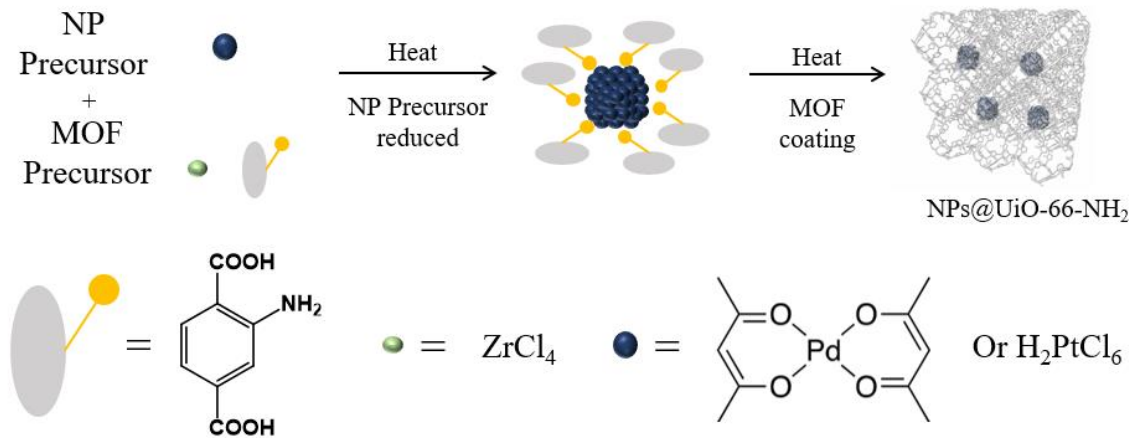
Figure 2.1 Scheme of one-pot synthesis of Pt/Pd @UiO-66-NH$_2$

2.2 Characterization of synthesized materials
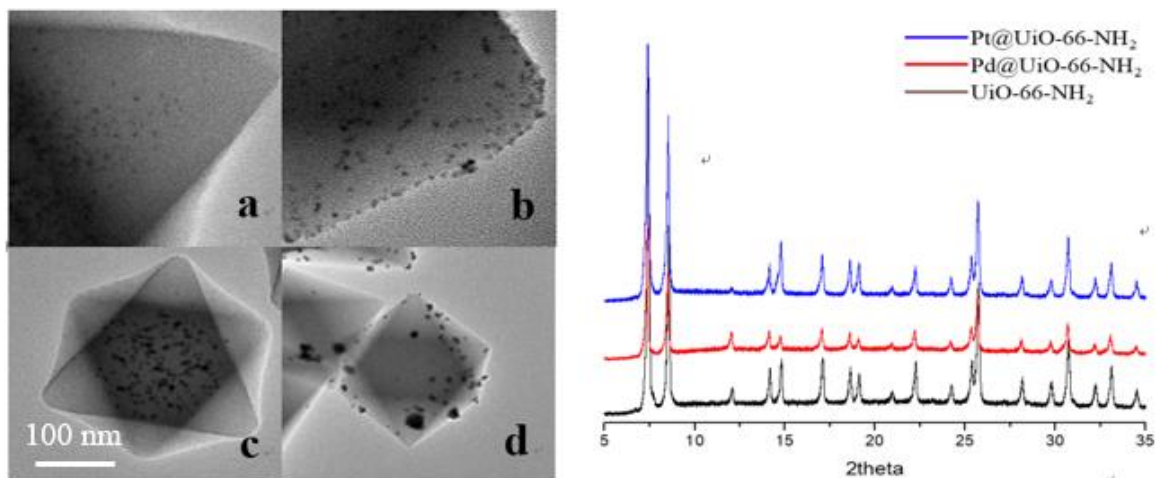
Figure 2.2 left side: TEM image of (a) Pt@UiO-66-NH$_2$ (b) Pt/UiO-66 (c) Pd@UiO-66-NH$_2$ (d) Pd/UiO-66 right side: XRD of Pt@UiO-66-NH$_2$, Pd@UiO-66-NH$_2$ and UiO-66-NH$_2$

As shown in the TEM images (**Figure 2.2 (a)(c)**), UiO-66-NH$_2$ forms very uniform octahedral particles with around 200-300nm diameter with many tiny metal nanoparticles inside. According to PXRD spectrum, synthesized Pt/Pd@UiO-66-NH$_2$ have the same

peaks as the intrinsic UiO-66-NH$_2$ which demonstrates that the coating MOF here still maintains the crystal structure.

2.3 Tuning synthetic conditions

The reaction time study (**Figure 2.3**) shows that formation process of the core-shell structure. TEM images of the synthetic solution at different reaction time were taken. At first, many metal nanoparticles generate in solution in 15 minutes while there is few MOF structure formed. When the reaction time goes to 45 minutes, MOFs start to form small spheres around metal NPs. After another 30 minutes, those spheres merge with each other and grow larger. The octahedral core-shell structures can already be recognized after reacting for 6.5 hours but the whole size is still smaller than the final product. The reaction time study demonstrates that the nucleation of metal nanoparticles and growth of MOFs outside the generated nanoparticles happen subsequently.
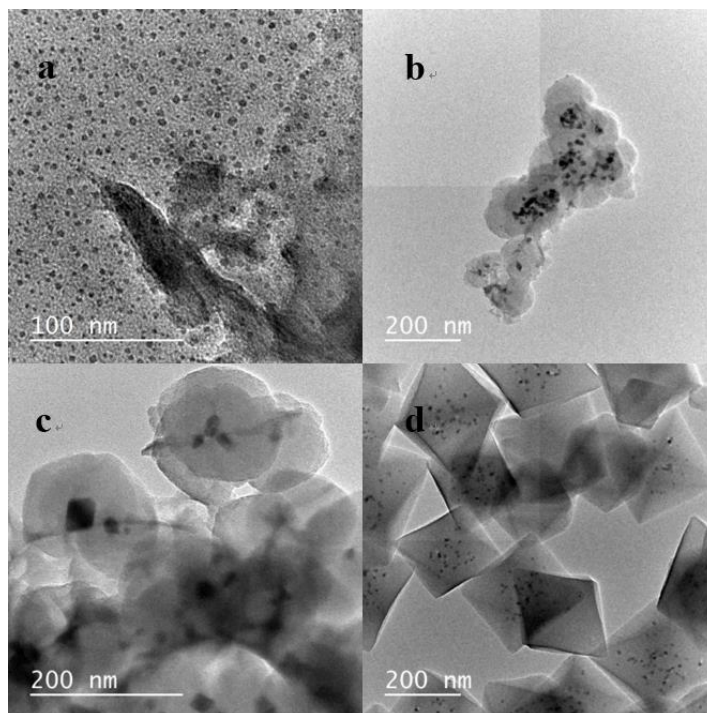
Figure 2.3 TEM images of Pd@UiO-66-NH$_2$ at different encapsulation time (a) 0.25h (b) 0.75h (c) 1.25h(d) 6.5h
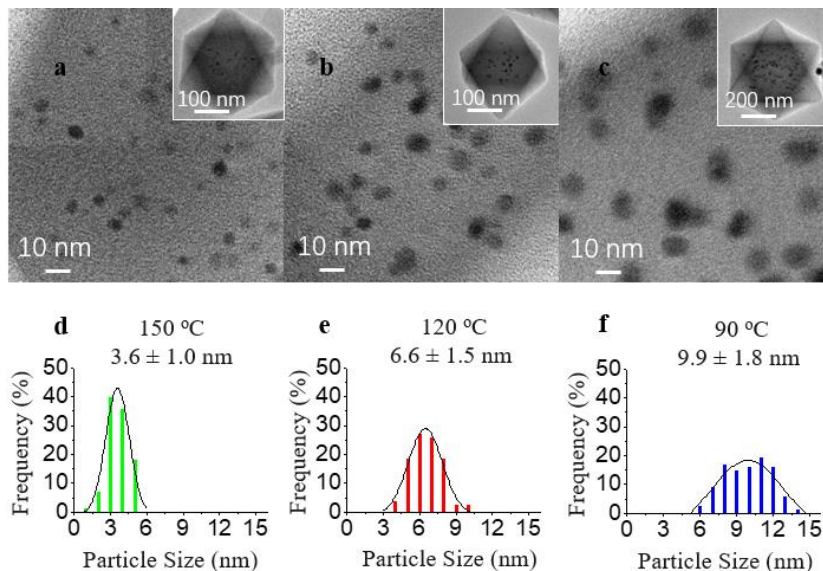
Figure 2.4 TEM images (upper) and particle size distribution (down, particle size collected manually) for Pd@UiO-66-NH$_2$ synthesized at different temperatures (a) (d)150 °C (b) (e)120 °C (c) (f) 90 °C

By varying the reaction temperature, we could tune the size of encapsulated metal nanoparticles (**Figure 2.4**). When the reaction temperature raises from 90 °C to 150 °C, the average size of Pd nanoparticles decreases from 9.9nm to 3.6nm. This trends can be explained by crystallization theory[16, 17], When the temperature goes higher, which means the increasing of supersaturation of metal in solution, the nucleation rate of nanoparticles will increase faster than growth rate of formed metal nanoparticle nucleus, which means more nanoparticle nucleus will form without further growth. Also, the faster formation of MOF shell outside nanoparticles will further restricts their growth. Additionally, by modifying the initial ratio of Pt/Pd precursors, we can get encapsulated Pt/Pd alloys with different elemental ratios. (**Table 1**)

19

As mentioned in chapter 1, not all nanoparticles@MOFs structure can be synthesized by one-pot method. Herein, we assume the interaction between aminol group on the NH_2-BDC linker and metal precursors plays an important role in the coating process. In order to verify our hypothesis, with BDC linker which has no amino group replacing original NH_2-BDC linker, the encapsulation reaction was repeated (**Figure 2.2** left (b)(d)). Not surprisingly, many metal nanoparticles without uniform size distribution formed outside the MOF particles, which provides a strong support to our hypothesis.

Sample	Pd (ppb)	Pt (ppb)	ICP (Pd:Pt) Molar ratio
Pd	2363	2.1	--
$Pd_{3.2}Pt_1$	1607	915.7	3.22
$Pd_{1.3}Pt_1$	1290	1767	1.34
$Pd_{0.7}Pt_1$	577	1472	0.72
Pt	27	2232	--

Table 1 Pd/Pt ration from different samples with different Pd/Pt precursor ratio (from ICP-OES)

2.4 Methods

General Considerations. Unless otherwise stated, all the reactions were carried out in the air without taking any precaution to protect reactions from oxygen or moisture. zirconium(IV) chloride ($ZrCl_4$, Aldrich, 99.5%), 2-aminoterephthalic acid (Aldrich, 99%), terephthalic acid (BDC, Sigma-Aldrich, 98%), acetic acid (Sigma-Aldrich, 99.7%), N,N-Dimethylformamide (DMF, Sigma-Aldrich, 99.8%), palladium(II) 2,4-

pentanedione (Pd(acac)$_2$, Alfa Aesar, Pd 34.7%), platinum(II) acetylacetonate (Pt(acac)$_2$, STREM CHEMICALS, 98%), Chloroplatinic acid hydrate (H$_2$PtCl$_6$, Sigma-Aldrich, 99.995%), Palladium(II) chloride (PdCl$_2$, Aldrich, 99%), ammonium tetrachloroplatinate(II) ((NH$_4$)$_2$PtCl$_4$, Sigma-Aldrich, 99%) were purchased from the indicated sources and used without further purification.

Scanning electron microscopy (SEM) was performed on a JOEL JSM6340F scanning electron microscope. Samples for SEM were prepared by diluting solid samples with 500 μL methanol and placing 2.0 μL droplet onto silica wafer and drying under a heat lamp. Transmission electron microscopy (TEM) was performed on a JEOL JEM2010F electron microscope operated at 200kV. Samples for TEM were prepared by diluting solid samples with 500 μL methanol and placing 2.0 μL droplets onto carbon-coated copper grids and drying under a heat lamp. The powder x-ray diffraction patterns (PXRD) were collected on a Bruker AXS diffractometer with Cu Kα radiation (λ= 1.5418 Å). Inductively coupled plasma optical emission (ICP-OES) spectrometry was recorded in an Agilent 5100 instrument that was calibrated using known concentrations of standard solutions to quantify Pt and Pd. Pt (1000 ppm), Pd (1000 ppm) single elemental standards were purchased from Inorganic Ventures.

Synthesis of UiO-66 and UiO-66-NH$_2$[2, 3]: In a typical synthesis reaction for UiO-66, 18.6 mg (0.08 mmol) ZrCl$_4$ and 13.3 mg (0.08 mmol) terephthalic acid were dissolved in 8.622 mL DMF, then 1.378 mL acetic acid was added into the solution to make the final volume to 10 mL. The solution was transferred into a 20mL scintillation vial and heated

for 24 hours in a 120 °C oil bath. After cooling down, the formed UiO-66 was collected by centrifugation. To form the UiO-66-NH$_2$, the same reaction parameters were followed, just with the use of 14.5 mg (0.08 mmol) 2-aminoterephthalic acid to obtain the functionalized MOF. The isolated samples were washed three times in methanol and dried under vacuum overnight.

Synthesis of Pd@UiO-66-NH$_2$ and Pd/UiO-66 composite: A typical synthesis reaction for Pd@UiO-66-NH$_2$ composite follows a similar procedure as the synthesis of UiO-66-NH$_2$; 8 x 10^{-3} mmol Pd(acac)$_2$ was dissolved in the DMF prior to the heating step. The reaction was then run for 24 hours at 120 °C and collected by centrifugation. To form the Pd/UiO-66 composite, the same reaction parameters were followed, just with the use of terephthalic acid instead of 2-aminoterephthalic acid. The isolated samples were washed three times in methanol and dried in a vacuum oven at 150 °C overnight.

Synthesis of Pt@UiO-66-NH$_2$ and Pt/UiO-66 composite: 18.6 mg (0.08 mmol) ZrCl$_4$, 14.5 mg (0.08 mmol) 2-aminoterephthalic acid and 8 x 10^{-3} mmol H$_2$PtCl$_6$ were dissolved in 8.622 mL DMF, then 1.378 mL acetic acid was added into the solution to make the final volume to 10 mL. The solution was transferred into a 20mL scintillation vial and heated for 24 hours in a 120 °C oil bath. After cooling down, the formed Pt@UiO-66-NH$_2$ was collected by centrifugation. To form the Pt/UiO-66 composite, the same reaction parameters were followed, just with use 13.3 mg (0.08 mmol) terephthalic acid. The isolated samples were washed three times in methanol and dried under vacuum overnight.

Digestion of Pt/Pd@UiO-66-NH₂ for ICP-OES analysis. Solid MOF material (5.00 mg) was weight out into a 1.5 mL Teflon vial. DMSO (300 µL) and 1 drop of 15 wt.% aqueous hydrofluoric acid solution was added in sequence. The mixture was sonicated for 1 minute and left to digest for 1 hour. The digested samples then heated to approximately 150 °C overnight in a sand bath open to the air to remove solvent. The resulting solid was dissolved and transferred to a 20 mL glass scintillation vial using a mixture (10% v/v) of hydrochloric acid in deionized water (300 µL). Each sample was diluted with additional deionized water (3.7 mL) and analyzed by ICP-OES.

2.5 Reference

1.   Chen, L., et al., *One-step encapsulation of Pd nanoparticles in MOFs via a temperature control program.* Journal of Materials Chemistry A, 2015. **3**(29): p. 15259-15264.

2.   Kandiah, M., et al., *Synthesis and Stability of Tagged UiO-66 Zr-MOFs.* Chemistry of Materials, 2010. **22**(24): p. 6632-6640.

3.   Ma, L., et al., *A series of isoreticular chiral metal–organic frameworks as a tunable platform for asymmetric catalysis.* Nature Chemistry, 2010. **2**(10): p. 838-846.

4.   Li, X., et al., *Controlling Catalytic Properties of Pd Nanoclusters through Their Chemical Environment at the Atomic Level Using Isoreticular Metal–Organic Frameworks.* ACS Catalysis, 2016. **6**(6): p. 3461-3468.

5.   Chen, L., et al., *Metal–organic framework encapsulated Pd nanoparticles: towards advanced heterogeneous catalysts.* Chemical Science, 2014. **5**(10): p. 3708-3714.

6.   Shi, J., et al., *Selective hydrogenation of cinnamaldehyde over reduced graphene oxide supported Pt catalyst.* Catalysis Communications, 2013. **41**: p. 101-105.

7. Chen, H., Z. Rui, and H. Ji, *Titania-supported Pt catalyst reduced with HCHO for HCHO oxidation under mild conditions.* Chinese Journal of Catalysis, 2015. **36**(2): p. 188-196.

8. Sui, X.-L., et al., *Investigation on C–TiO2 nanotubes composite as Pt catalyst support for methanol electrooxidation.* Journal of Power Sources, 2014. **255**: p. 43-51.

9. Chao, G., et al., *Electron-rich platinum electrocatalysts supported onto tin oxides for efficient oxygen reduction.* Composites Communications, 2021. **24**: p. 100603.

10. Zhang, Y. and J. Zhou, *Synergistic catalysis of hybrid nano-structure Pt catalyst for high efficiency selective hydrogenation of nitroarenes.* Journal of Catalysis, 2021.

11. Albinsson, D., et al., *Shedding Light on CO Oxidation Surface Chemistry on Single Pt Catalyst Nanoparticles Inside a Nanofluidic Model Pore.* ACS Catalysis, 2021: p. 2021-2033.

12. Etemadi-Davan, E., et al., *Palladium nanoparticles on amino-modified silica-catalyzed C–C bond formation with carbonyl insertion.* Journal of the Iranian Chemical Society, 2021.

13. Kitagawa, O., *Chiral Pd-Catalyzed Enantioselective Syntheses of Various N–C Axially Chiral Compounds and Their Synthetic Applications.* Accounts of Chemical Research, 2021. **54**(3): p. 719-730.

14. Crombie, C.M., et al., *The Selective Oxidation of Cyclohexane via In-situ H2O2 Production Over Supported Pd-based Catalysts.* Catalysis Letters, 2021.

15. Hu, M., et al., *N8 stabilized single-atom Pd for highly selective hydrogenation of acetylene.* Journal of Catalysis, 2021. **395**: p. 46-53.

16. Lutsko, J.F., *How crystals form: A theory of nucleation pathways.* Science Advances, 2019. **5**(4): p. eaav7399.

17. Tsukimura, K., et al., *Kinetic Theory of Crystallization of Nanoparticles.* Crystal Growth & Design, 2010. **10**(8): p. 3596-3607.

Chapter 3 Hydrogenation of Crotonaldehyde

3.1 Introduction

As mentioned in Chapter 2, Pt/Pd@UiO-66-NH$_2$ have been successfully synthesized via

one pot method and characterized. With the clean surface and well-controlled size and

wide catalytic application spectrum of Pt/Pd nanoparticles, our materials are expected to

have above-average level of catalytic performance, without mentioning the uniform pores

in shell MOFs. Herein, selective hydrogenation of α, β-unsaturated aldehyde was selected

to demonstrate the catalytic performance of our catalysts.

3.2 Selective Hydrogenation of α, β-Unsaturated Aldehyde
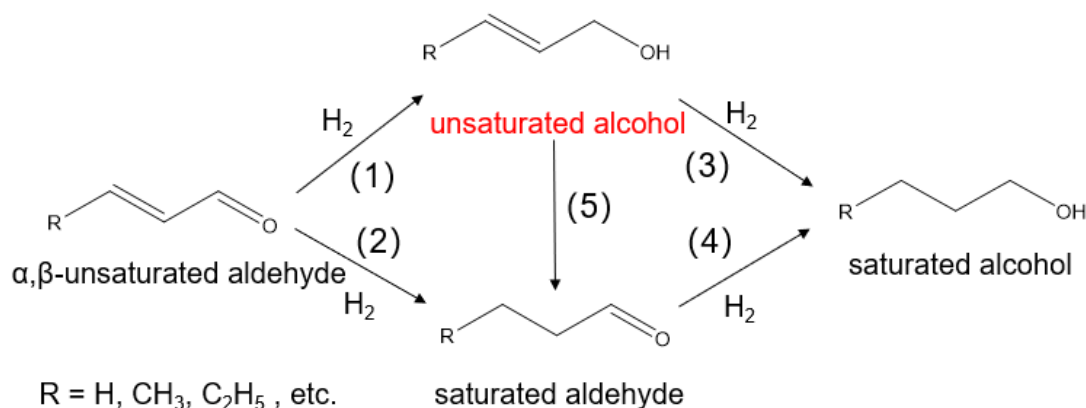
Figure 3.1 reaction pathways of α, β-unsaturated aldehyde hydrogenation

It is an important step in industry to selective catalytically hydrogenate organic substrates

with more than one unsaturated functional groups, which also draws a lot of attentions in

fundamental research.[1-11] For example, unsaturated alcohols from hydrogenation of

the carbonyl groups of α, β-unsaturated aldehydes are valuable products in industry which can be used to make perfumes, flavoring and pharmaceuticals. However, in the presence of most traditional group VIII metal catalysts, α, β-unsaturated aldehydes are hydrogenated mainly to saturated aldehydes by reduction of the C=C group or fully hydrogenated to saturated alcohols. [1, 4]Therefore, it is highly desired to find a catalyst which can hydrogenate the carbonyl group effectively while keep the C=C double bond intact. (**Figure 3.1**, reaction 1 vs. 2).

Furthermore, in order to prevent fully hydrogenation to the saturate alcohol (**Figure 3.1**, reactions 3 and 4) and isomerization of the unsaturated alcohol (**Figure 3.1**, reaction 5), the catalyst must suppress these reaction pathways. Even all the pathways in figure 3.1 are thermodynamically possible, the C=C double bond in α, β-unsaturated aldehyde is still more active and easier to be reduced than the C=O double bond. Thus, selectivity to unsaturated alcohol must be achieved by modifying the rate constants of two competitive reactions and the adsorption constants of the substrates.

A lot of attempts have been made to develop a suitable catalytic system. And a huge part of previous works are based on transition metals like Pt/Pd. [3, 8, 12-14]According to previous works and thermodynamic and kinetic analysis, comparing to Pd-based catalysts, carbonyl group will be more active on Pt-based ones which means the selectivity towards unsaturated alcohol will be higher.[2, 4, 5] While C=C double bond is so active for Pd-based catalysts that it is not hard to achieve 99% selectivity for sutured

aldehyde.[15, 16] It is worth nothing that our results match with those experimental and theoretical results, which will be discussed later in this chapter.

3.3 Spatial Confinement of MOF
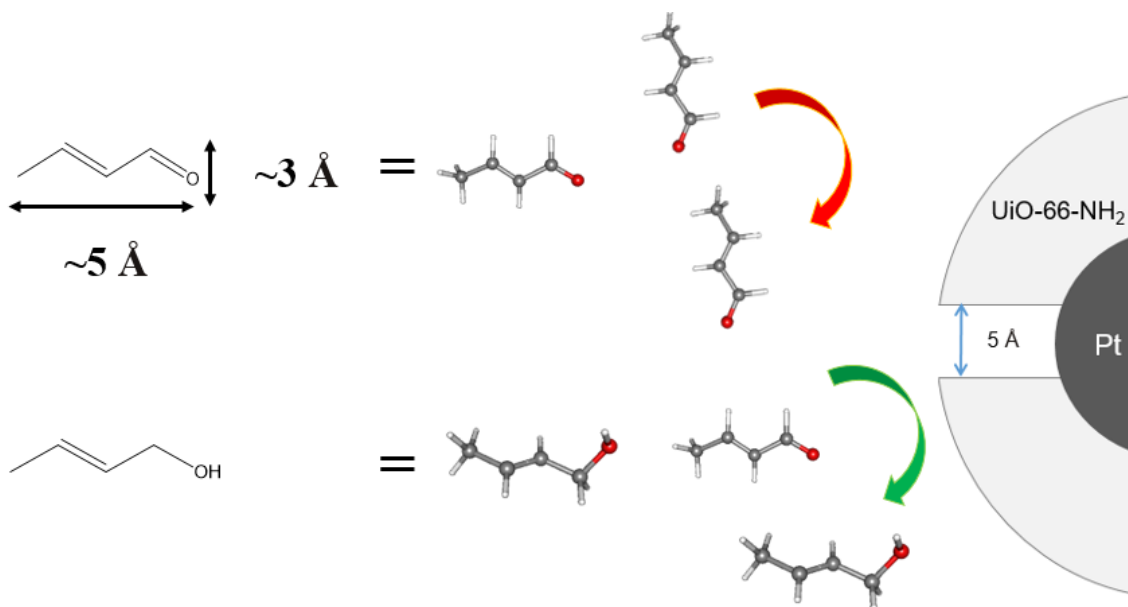
Figure 3.2 spatial confinement of MOFs for reactant crotonaldehyde attaching to NP surface

For our catalysts, we choose crotonaldehyde which has a suitable size to test the catalytic performance of our Pt/Pd@UiO-66-NH$_2$ sample. We believe that the uniform channels in MOF crystal can provide a spatial confinement for the chosen reaction. The aperture size of the octahedron cages in UiO-66 is 5Å, which is a bit smaller than the axial length of Crotonaldehyde but larger than the width of the substrate molecule, which means the orientation that the substrate molecules get close to the active sites on nanoparticle surface is limited. Generally, two ends of the substrate molecules are more likely to get close to the active sites, which means the carbonyl group is more likely to be activated

and reduced (Down side of **Figure 3.2**) while the steric hinder from methyl group in C=C double bond suppress the 3,4-reduction. Additionally, the chain length of crotonaldehyde is larger than the aperture size, which means the 1,4-absorption and further 1,4-reduction are less likely to occur. (Upper side of **Figure 3.2**) In conclusion, due to the spatial confinement of MOF, 2-Butenol, the product come from 1,2-reduction, is expected to be the main product, which is exactly what we want.[14, 17]

3.4 Determination of Reaction Condition

For Crotonaldehyde, the substrate we choose to test the catalytic performance of our Pt@UiO-66-NH$_2$ sample, the three possible reduction products of it are Butyraldehyde, Butanol and 2-Butenol (Upper side of **Figure 3.3**). Among these products, 2-Butenol is our target product. The liquid phase hydrogenation reaction is performed in a 500 mL stainless steel Parr reactor pressurized with pure H$_2$ gas. A thermocouple inside the reactor chamber and a hot plate underneath are utilized to ensure thermostatic reactions. Substrate, catalyst, isopropanol solvent and a magnetic stir bar are mixed in ampules which are put into the reactor chamber to run parallel reactions. (Down side of **Figure 3.3**)

Before performing further experiments, we do the reaction condition scanning and choose 3Mpa H$_2$ pressure, 70 °C reaction temperature and reaction time of 18 hours for all control experiments. Under these reaction conditions, our core-shell Pt@UiO-66-NH$_2$ shows best catalytic performance. Interestingly, our Pd@UiO-66-NH$_2$ shows pretty high selectivity towards Butyraldehyde with high activity, which matches with previous experimental and theoretical results that Pd catalyst has superior activity and selectivity

28

of reduction of C=C double bond. [2, 15]As Pd-based catalyst is not suitable for selective

hydrogenation of carbonyl group, all the following experiments are about Pt-based ones.

Since conversion of the reaction will also influence the selectivity, we tune the amount of

each catalyst to make sure all the reactions stop at 30% conversion to make results

comparable. Catalysts amount required to reach 30% selectivity are used to compare their

relative activity. (**Table 2**)
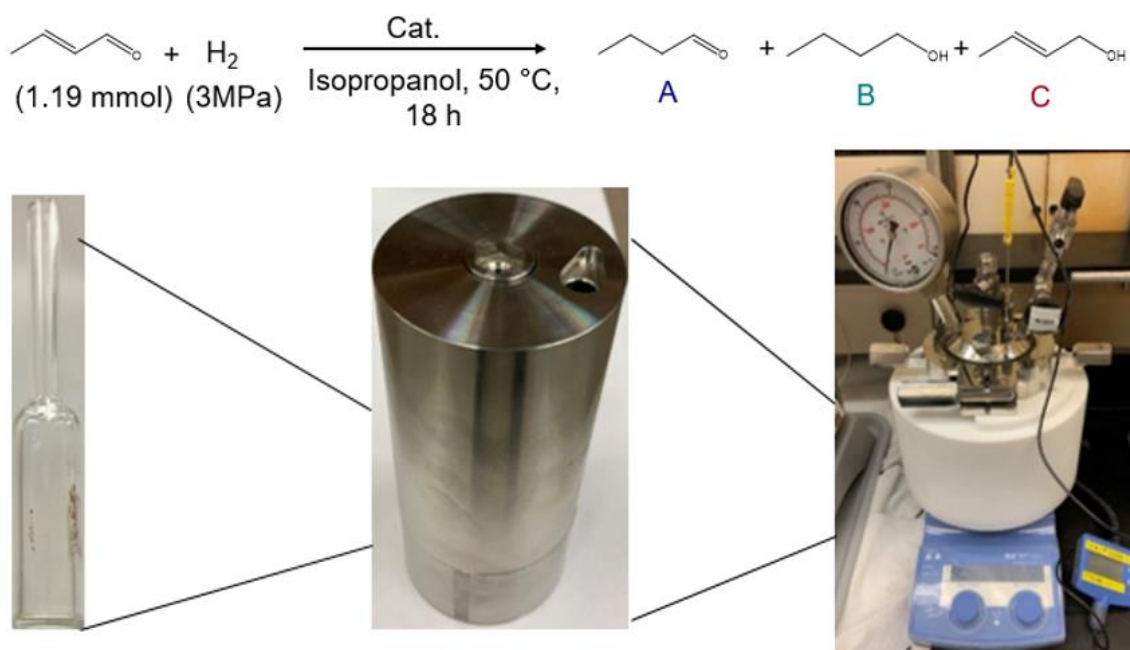
Figure 3.3 Upper side**:** Hydrogenation of Crotonaldehyde and three major products A

Butyraldehyde B Butanol C 2-Butenol. Down side: reaction apparatus set up.

3.5 Catalytic Performance

At the very beginning, 5% Pt/SiO$_2$ as a commercial catalyst is firstly applied in our

reaction system to test our reactor and serves as a standard. Not surprisingly, Pt/SiO$_2$

catalyst shows low selectivity to our desired product (32.43% of 2-Butenol) but more

likely to form Butyraldehyde (53.60%). As we mentioned before, C=C double bond is

more active and more likely to be reduced by H_2. The product distribution here matches with literature reported and theoretical analysis [2-4, 15] Interestingly, commercial Pt/SiO$_2$ shows the highest activity except for our one-pot Pt@UiO-66-NH$_2$(**Table 2**), which makes sense especially when thinking about the diffusion barrier comes from PVP and/or coating MOFs in other cases.
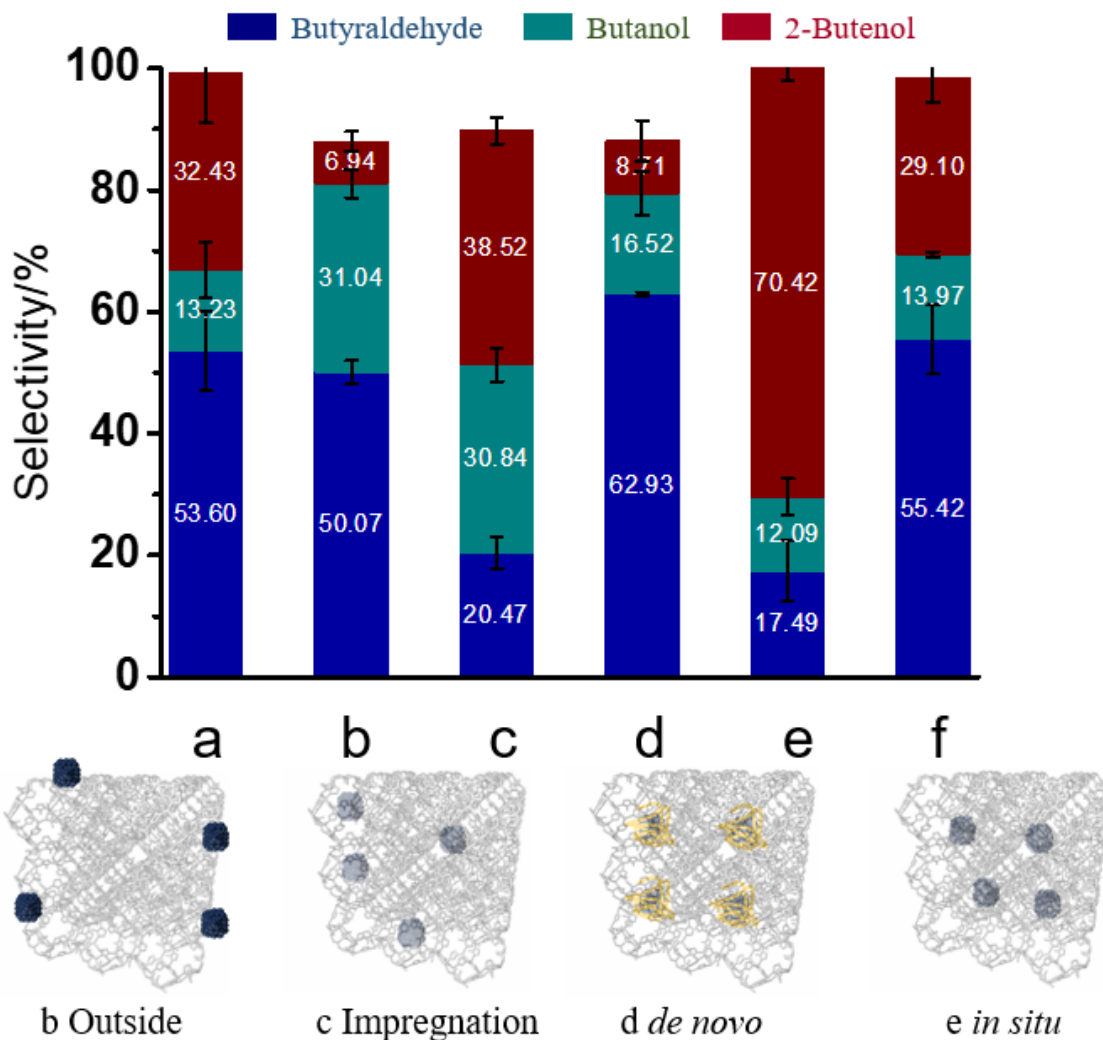
Figure 3.4 Catalytic performance of (a) commercial Pt/SiO$_2$ (b) outside physical mixture of Pt (PVP) with UiO-66-NH$_2$ (c) Impregnation Pt@UiO-66-NH$_2$ synthesized via post impregnation approach (d) *de novo* Pt@UiO-66-NH$_2$ synthesized via *de novo* approach (e) *in situ* Pt@UiO-66-NH$_2$ synthesized via one-pot approach (f) Pt/SiO$_2$ with PVP

Sample	Pt amount (mg)	Relative activity
Pt/SiO$_2$	0.2	1
Pt/SiO$_2$ with PVP	0.5	0.40
Pt@UiO-66-NH$_2$	0.06	3.33
Pt(PVP)@UiO-66-NH$_2$	0.60	0.33
Pt/UiO-66-NH$_2$	0.30	0.67
Pt(PVP)/UiO-66-NH$_2$	0.60	0.33

Table 2 catalysts amount required to achieve 30% conversion under our reaction conditions and relative activity comparing to commercial Pt/SiO$_2$

In order to confirm the clean surface of our one-pot *in situ* synthesized Pt@UiO-66-NH$_2$, we did several control experiments. First of all, we need to make sure that surface-attached PVP do have a negative influence on the catalytic performance of Pt catalysts. We use PVP to "poison" the merchant Pt/SiO$_2$ catalyst, and compare its catalytic performance to the original one. According to the average of 3 trials, PVP "poisoned" Pt/SiO$_2$ shows a 60% decrease in activity while its selectivity also decreases. (**Table 2**)

This control experiment successfully demonstrates that PVP on the surface of Pt catalyst will dramatically depress the activity and significantly influence the selectivity.

Based on this result, we designed another control experiment. Our catalyst has a pretty fine selectivity towards our target product which is 70.42%, meanwhile, Pt (PVP)@UiO-66-NH$_2$ synthesized via ship around bottle approach only has about 8.71% selectivity and the latter one also has 10 times lower activity comparing to the former one. We believe the main difference of those two Pt-MOF core-shell nanoparticles is that Pt (PVP) one is synthesized via de novo approach, since Pt nanoparticles are formed in PVP solutions and stabilized by it, so it is nearly impossible to remove all the attached PVP during the coating of MOF, and those PVP will wrap those Pt nanoparticles and block lots of active sites.

MOFs around nanoparticles not only played the role of capping agent during the synthesized, their limited pore size also provided a kind of size effect so that the reactant can only pass through it when the molecule is parallel with the channel, so that the carbonyl end will more likely get close to the active sites on Pt surface and the reaction will happen in our preferred way. In order to test this hypothesis, we simply mix Pt nanoparticles and UiO-66-NH$_2$ particles and this Pt/UiO-66-NH$_2$ physical mixture shows the lowest selectivity in all samples-only 6.9%, while the coated one is 10 times higher. We believe this mainly comes from lacking of the size confinement effect of MOFs.

Before we also mentioned about ship in a bottle approach. So, we also synthesized a sample via impregnation approach. This one has a 38.5% selectivity which is half of our sample but much better than outside ones and de novo ones, which is reasonable because in this one the size effect should also work. However, we believe that a part of Pt nanoparticles may formed on the surface of MOFs instead of inside during the reduction process and these Pt nanoparticles contribute to the low selectivity. Also, a better sharp and size control of our one-pot method may also take part in this, but we still need more evidence to support this hypothesis.

3.6 Conclusion

In the chapter, we compare catalytic performance of our one-pot synthesized Pt@UiO-66-NH2 of selective hydrogenation of α, β-unsaturated aldehyde with commercial Pt catalysts and NP/MOF composites synthesized via other approaches. Among all these samples, the highest activity and selectivity of our sample demonstrates the advantages of clean surfaces and spatial confinement. This experimental result matches with the theoretical calculation that only a well-defined direct contact interface of metal nanoparticles and MOF could provide this spatial confinement to improve the selectivity towards unsaturated alcohols. [2, 9] However, what happens in the nanoparticles and MOF interface and the role of side chain functional group of the organic linker- amine group during the reaction are still unclear. In order to dig deeper in this question, we need alter the side chain of the BDC-NH$_2$ linker and test catalytic performance.

3.7 Methods

General Considerations. Unless otherwise stated, all the reactions were carried out in the air without taking any precaution to protect reactions from oxygen or moisture. zirconium(IV) chloride (ZrCl$_4$, Aldrich, 99.5%), 2-aminoterephthalic acid (Aldrich, 99%), acetic acid (Sigma-Aldrich, 99.7%), N,N-Dimethylformamide (Sigma-Aldrich, 99.8%), palladium(II) 2,4-pentanedione (Pd(acac)$_2$, Alfa Aesar, Pd 34.7%), Platinum(II) acetylacetonate (Pt(acac)$_2$, STREM CHEMICALS, 98%), Chloroplatinic acid hydrate (H$_2$PtCl$_6$, Sigma-Aldrich, 99.995%), Palladium(II) Chloride (PdCl$_2$, Aldrich, 99%), ammonium tetrachloroplatinate(II) ((NH$_4$)$_2$PtCl$_4$, Sigma-Aldrich, 99%), Sodium hydroxide (NaOH, Sigma-Aldrich, 98%), polyvinylpyrrolidone (PVP, Mw~40,000, Aldrich), tetramethylammonium bromide (N$^+$(CH$_3$)$_4$Br$^-$, Sigma-Aldrich, 99%), crotonaldehyde (predominantly trans, Sigma-Aldrich, >99%), 3-Buten-1-ol(Sigma-Aldrich, 96%), 1-Butanol(anhydrous, Sigma-Aldrich, 99.8%), Butyraldehyde(anhydrous, Sigma-Aldrich, >99%), Isopropyl alcohol(Sigma-Aldrich, 98%), Diethyl Ether (Supelco), Dimethyl sulfoxide-d$_6$(DMSO-d$_6$, Sigma-Aldrich, 99.8% D), Hydrofluoric acid (HF, Supelco, 48%) were purchased from the indicated sources and used without further purification. Hydrogen (Airgas, 99.999%) and Nitrogen (Airgas, 99.999%) were used for heterogeneous catalysis.

^{1}H Nuclear magnetic resonance (NMR) spectroscopy was performed on Varian 500 MHz and 600 MHz NMR spectrometers. Tetramethylsilane ((CH$_3$)$_4$Si: 0.0 ppm) was used as an internal reference for ^{1}H NMR spectra. Samples were prepared by digesting approximately 10 mg of UiO-66 or linker-exchanged UiO-66 samples with sonication in

580 µL of DMSO-d_6 and 20 µL of HF (48% aqueous solution). All of the NMR measurements were performed with 90- degree pulse and a recycle delay larger than 5 times of spin-lattice relaxation time between each transient to ensure complete relaxation of the observed spins.

Synthesis of PVP Capped 5 nm Pt Nanocrystals: The synthesis was carried out following the previous report with slight modifications.[18] A total of 0.025 mmol of Pt ions $(NH_4)_2PtCl_4$, 0.75 mmol of tetramethylammonium bromide, and 0.5 mmol of polyvinylpyrrolidone (in terms of the repeating unit; Mw 40 000) were dissolved into 5 mL of ethylene glycol in a 25 mL round-bottom flask at room temperature. The mixed solution was stirring and heated to 200°C in an oil bath for 20 minutes.

Synthesis of PVP coated 5nm Pt NPs@UiO-66-NH₂ composite: Following a similar procedure as the synthesis of UiO-66-NH₂, another 1 mL of 0.25 mg/mL of the DMF solution of PVP capped Pt particles was added to the UiO-66-NH₂ synthetic solution to make the final volume to 10 mL. The solution was transferred into a 20mL scintillation vial and heated for 24 hours in a 120 °C oil bath. The isolated samples were washed three times in methanol and dried in a vacuum oven at 150 °C overnight.

Synthesis of "Unprotected" Pt Nanoclusters: Pt nanoparticles were synthesized according to literature.[19] In a typical preparation, a glycol solution of NaOH (50 mL, 0.5 M) was added into a glycol solution of $H_2PtCl_6.6H_2O$ (1.0 g, 1.93 mmol in 50 mL) with stirring to obtain a transparent yellow platinum hydroxide or oxide colloidal solution which was then heated at 160 °C for 3 h, with a N_2 flow passing through the reaction

system to take away water and organic byproducts. Then add a dilute aqueous solution of HCl to adjust pH of the Pt nanocluster solution to a value lower than 4. The isolated samples were washed three times in methanol and dispersed in 10mL of methanol.

Synthesis of "Unprotected" Pt NPs/UiO-66-NH₂ composite: 40 mg of as synthesized UiO-66-NH₂ was add to 16 mL of methanol, then the mixture was sonicated for 10 minutes. Under stirring, 4 mL of 0.3 mg/mL of the methanol solution of "unprotected" Pt particles was added drop by drop. After that, keep stirring for 120 minutes. Then formed "Unprotected" Pt NPs/UiO-66-NH₂ composite was collected by centrifugation. The isolated samples were washed three times in methanol and dried under vacuum overnight.

Preparation of Pt/SiO₂ with PVP: 100mg 5% Pt/SiO₂ was added to 10ml PVP aqueous solution with 100mg PVP. The solution was sonicated and then stirred overnight. Then treated Pt/SiO₂ were collected by centrifugation. The isolated samples were washed three times in ethanol and dried under vacuum overnight.

Selective hydrogenation of crotonaldehyde: In a typical procedure, a certain amount of catalyst was dispersed in 2.4 mL isopropanol solution, and 100 μL trans-crotonaldehyde (1.19 mmol, Aldrich >99%) were added into the above solution. Subsequently, the solution was transferred into a 4.0-mL ampule using a 9" glass pipet. These ampules were arranged in a 500 mL stainless steel Parr reactor that contained a thermocouple to ensure thermostatic reactions. The reactor was placed on the top of a Ika RCT-basic hot plate. The reactor vessel was purged with H₂ for 3 times, and the final H₂ pressure of the vessel

was set at 3.0 MPa. During the catalytic process, the reaction solution was magnetically stirred with the speed of 800 rpm at desired temperature for the 18 hours.

After that, the catalysts were separated by centrifugation, and the obtained reaction solution was analyzed by gas chromatography-mass spectrometry (GC-MS, Shimadzu, GC-MS-QP2010 Ultra, column: SH-Rtx-Wax, 60 m × 0.25 mm × 0.5μm)

Reaction system analysis:

Firstly, we use ^{1}H-NMR to analysis the reaction system to get the percentage of different products. However, due to the limitation of NMR, sometimes we will get different results when choosing different peak areas to calculate. Also, some of those peaks are collapsed and the whole graph become so difficult to read. In order to get more reliable and precise results, we start to use GC-MS to analysis and get pretty good results. (**Figure** 3.5)
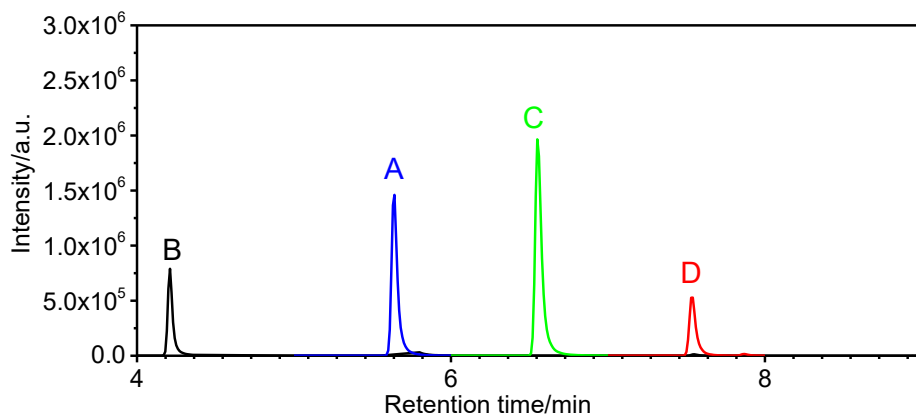
Figure 3.5 GC-MS spectrum of the mixture of reactant and 3 products, all peaks are separated clearly. A Crotonaldehyde, B Butyraldehyde, C Butanol, D 2-Butenol

The reaction solution was analyzed by gas chromatography-mass spectrometry (GC-MS, Shimadzu, GC-MS-QP2010 Ultra, column: Rtx-Wax, 60 m × 0.25 mm × 0.5μm). Typically, a 100 μL of reaction solution was diluted by 9.90mL of ethyl ether. Then 10 μL of diluted solution was injected into GC-MS manually and run the process with following parameters **(Table 2)**

The MS detector works in Scan and SIM mode so it gives out two chromatographs, one (from Scan mode) counts every fraction with m/z between 40-150, the other (from SIM mode) only counts fractions with several m/z (56 70 72). Quantified analysis mainly based on the second mode.

GC-MS parameters	Value
Column Oven Temp	70.0 °C
Injection Temp	250.00 °C
Injection Mode	Split
Flow Control Mode	Linear
Velocity Pressure	24.3 kPa
Total Flow	58.2 mL/min
Column Flow	9.62 mL/min
Linear Velocity	113.7 cm/se c
Purge Flow	0.5 mL/min
Split Ratio	5.0
Temperature program	70-240 °C 10 °C /min

Table 3 GC-MS parameters

Determination of Calibration Curves:

Before analyzing the reaction solution, we need to build calibration curve using

standards. Standards of reactants and products (Crotonaldehyde, Butyraldehyde, Butanol,

2-Butenol) with certain concentrations were analyzed by GC-MS separately and together.

From the GC-MS spectrum, we can see that all 4 peaks are separated pretty well with no

overlapping with each other and their retention times maintain stable which means GC-

MS can be used to analyze reaction solution.

All standards are made by series dilution from a storage solution. A series of amounts

(0.1-100μL) of standards (Crotonaldehyde, Butyraldehyde, Butanol, 2-Butenol) were

diluted with reaction solvent (isopropanol) to 2.5mL, then 100μL mixed solutions were

taken out and diluted by 9.90mL of diethyl ether. Then as-prepared diethyl ether

solutions were analyzed by GC-MS. For each standard (reactant or products), at least 7

different concentrations were tested to make sure their GC-MS peak areas have good

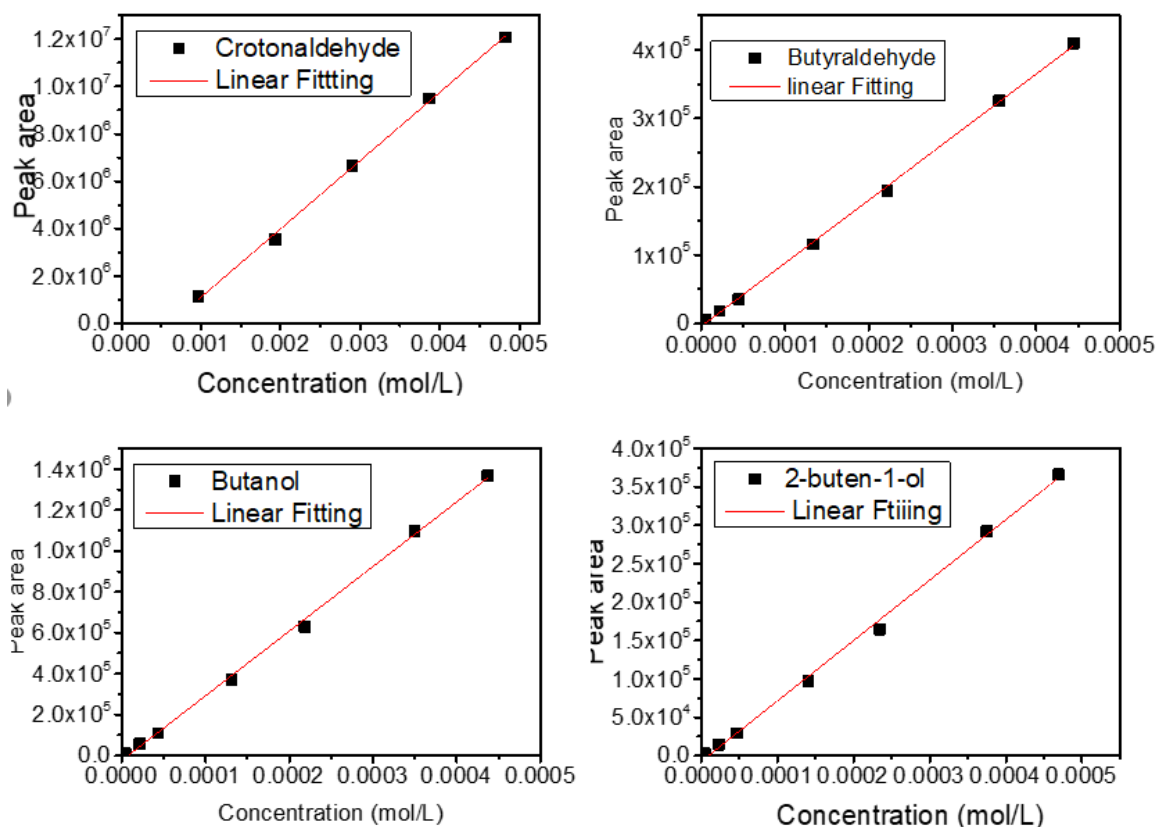liner relation shape with their concentrations. (**Figure 3.6**)

Figure 3.6 Calibration curves of the reactant and 3 products, all R^2 are larger than 0.99.

a）Crotonaldehyde, b) Butyraldehyde, c) Butanol, d) 2-Buten-1-Ol

3.8 Reference

1. Raab, C.G., et al., *Selective Hydrogenation of Crotonaldehyde over Pt Derived Catalysts*, in *Heterogeneous Catalysis and Fine Chemicals III, Proceedings of the 3rd International Symposium*. 1993. p. 211-218.

2. Delbecq, F. and P. Sautet, *Competitive C——C and C——O Adsorption of α-β-Unsaturated Aldehydes on Pt and Pd Surfaces in Relation with the Selectivity of Hydrogenation Reactions: A Theoretical Approach.* Journal of Catalysis, 1995. **152**(2): p. 217-236.

3. Claus, P., *Selective hydrogenation of ά,β-unsaturated aldehydes and other C=O and C=C bonds containing compounds.* Topics in Catalysis, 1998. **5**(1): p. 51-62.

4. Cao, X.-M., et al., *Reaction Mechanisms of Crotonaldehyde Hydrogenation on Pt(111): Density Functional Theory and Microkinetic Modeling.* The Journal of Physical Chemistry C, 2011. **115**(40): p. 19819-19827.

5. Jesús, J.C.d. and F. Zaera, *Adsorption and thermal chemistry of acrolein and crotonaldehyde on Pt(111) surfaces.* Surface Science, 1999. **430**(1-3): p. 99-115.

6. Blackmond, D.G., et al., *Geometric and electronic effects in the selective hydrogenation of α, β-unsaturated aldehydes over zeolite-supported metals.* 1991. **131**(2): p. 401-411.

7. Tian, et al., *Highly chemoselective hydrogenation of crotonaldehyde over Ag-In/SBA-15 fabricated by a modified "two solvents" strategy.* Chemical communications (Cambridge, England), 2011. **47**(21): p. 6168-70.

8. Zhao, M., et al., *Metal–organic frameworks as selectivity regulators for hydrogenation reactions.* Nature, 2016. **539**(7627): p. 76-80.

9. Tian, Z., et al., *Theoretical Evidence on the Confinement Effect of Pt@UiO-66-NH2 for Cinnamaldehyde Hydrogenation.* The Journal of Physical Chemistry C, 2019. **123**(36): p. 22114-22122.

10. Tamura, M., et al., *Selective Hydrogenation of Crotonaldehyde to Crotyl Alcohol over Metal Oxide Modified Ir Catalysts and Mechanistic Insight.* ACS Catalysis, 2016.

11. Yuan, K., et al., *Effective and Selective Catalysts for Cinnamaldehyde Hydrogenation: Hydrophobic Hybrids of Metal‐Organic Frameworks, Metal Nanoparticles, and Micro‐ and Mesoporous Polymers.* Angewandte Chemie, 2018. **130**(20).

12. Zhang, W., et al., *Site-Selective Catalysis of a Multifunctional Linear Molecule: The Steric Hindrance of Metal-Organic Framework Channels.* Advanced Materials, 2018. **30**(23).

13. Lan, X., et al., *Geometric effect in the highly selective hydrogenation of 3-methylcrotonaldehyde over Pt@ZIF-8 core–shell catalysts.* Catalysis Science & Technology, 2017. **7**(12): p. 2601-2608.

14. Guo, Z., et al., *Pt Nanoclusters Confined within Metal–Organic Framework Cavities for Chemoselective Cinnamaldehyde Hydrogenation.* ACS Catalysis, 2014. **4**(5): p. 1340-1348.

15. Nagendiran, A., et al., *Mild and Selective Catalytic Hydrogenation of the C=C Bond in alpha,beta-Unsaturated Carbonyl Compounds Using Supported Palladium Nanoparticles.* Chemistry, 2016. **22**(21): p. 7184-9.

16. Zhao, F., et al., *An effective and recyclable catalyst for hydrogenation of α,β-unsaturated aldehydes into saturated aldehydes in supercritical carbon dioxide.* Green Chemistry, 2003. **5**(1): p. 76-79.

17. Wu, B., et al., *Selective hydrogenation of alpha,beta-unsaturated aldehydes catalyzed by amine-capped platinum-cobalt nanocrystals.* Angew Chem Int Ed Engl, 2012. **51**(14): p. 3440-3.

18. Tsung, C.-K., et al., *Sub-10 nm Platinum Nanocrystals with Size and Shape Control: Catalytic Study for Ethylene and Pyrrole Hydrogenation.* Journal of the American Chemical Society, 2009. **131**(16): p. 5816-5822.

19. Wang, Y., et al., *Preparation of Tractable Platinum, Rhodium, and Ruthenium Nanoclusters with Small Particle Size in Organic Media.* Chemistry of Materials, 2000. **12**(6): p. 1622-1627.

Chapter 4 Linker exchange

4.1 Introduction

In the former chapter, selective hydrogenation of crotonaldehyde was applied to test the catalytic performance of our one-pot synthesized Pt @UiO-66-NH_2 catalyst and the results proof the existence of well-defined direct contact interface of metal and MOF and spatial confinement comes from MOF. We believe the NH_2 group in NH_2-BDC played an important role in the formation of Pt nanoparticle and coating of MOFs and the experiment replacing NH_2-BDC with BDC provided a strong support on it. However, when the whole synthesis process is done, will the NH_2 group still bond to the Pt atoms and will this interaction affect their catalytic performance? The steric and electronic effect of side chain functional group in MOF linker and it influence to the catalytic performance are still unclear. In order to explore this question, we need to get the same structure with removing or replacing the amine group and run the same reaction. However, as shown in **Figure 2.2**, Pt nanoparticles cannot be encapsulated into MOFs without amine group, which means Pt@UiO-66 with a replaced functional group cannot be directly manufactured by our one-pot method. Likely, the similarity between MOFs and conventional coordination compounds provides us another approach: Post synthetic linker exchange which allows to achieve our desired structures. (see 4.2)

In this part of the thesis, we discussed the influence of the side chain of BDC linker to the catalytic performance of our Pt@UiO-66-NH_2 samples. Linker exchange were utilized to replace the NH_2-BDC linkers while maintain its topology.

4.2 Postsynthetic Linker Exchange

Thanks to the coordination-driven self-assemble properties of MOFs, rational design of MOFs can be accessed via judicious choosing of secondary building units and organic linkers, achieving desired topologies and properties in a convenient and facile one-step synthesis. However, there are still some MOF structures cannot be directly produced in such "one-step" process, including the ones with incompatible motifs in reaction conditions. Also, undesired side products are sometimes generated because of the existence of several stable or sub stable structures for similar chemical components or catenation. Due to such shortcomings of conventional "one-step" synthesis, postsynthetic modification (PSM) in MOFs (e.g., protection and deprotection of active functional groups, and further modification of functional groups) was developed by scientists to expand the reachable range of MOF structures and components. This methodology shows the possibility of taking MOFs as "molecules".

Based on this concept, a new synthetic strategy, postsynthetic linker exchange (PSLE), also known as solvent-assisted linker exchange, was developed. Just like well-developed linker exchange strategy in coordination compounds, post synthetic linker exchange of MOFs is initiated by merging an existing MOF to a concentrated solution of a new linker. (**Figure 4.1**) Unlike the homogenous process of traditional homogenous process of coordination compounds, this heterogeneous reaction can partially or entirely exchange the structural linkers in pristine MOFs while maintains the topology of it. Nowadays, PSLE has already been successfully applied in numerous types of MOFs, even some extremely chemically stable and robust ones (e.g., UiO (University of Oslo, the

institution where the first UiO MOF was created) series discussed in this thesis), and leading to the formation of MOFs that had been challenging to prepare directly. PSLM can be used to (i) synthesize new MOFs or introduce new chemical functionalities in MOFs (which may not be accessible de novo), (ii) control pore size/shape, (iii) control catenation, and (iv) access topologies that are unknown for a particular linker/node combination.[1-6]
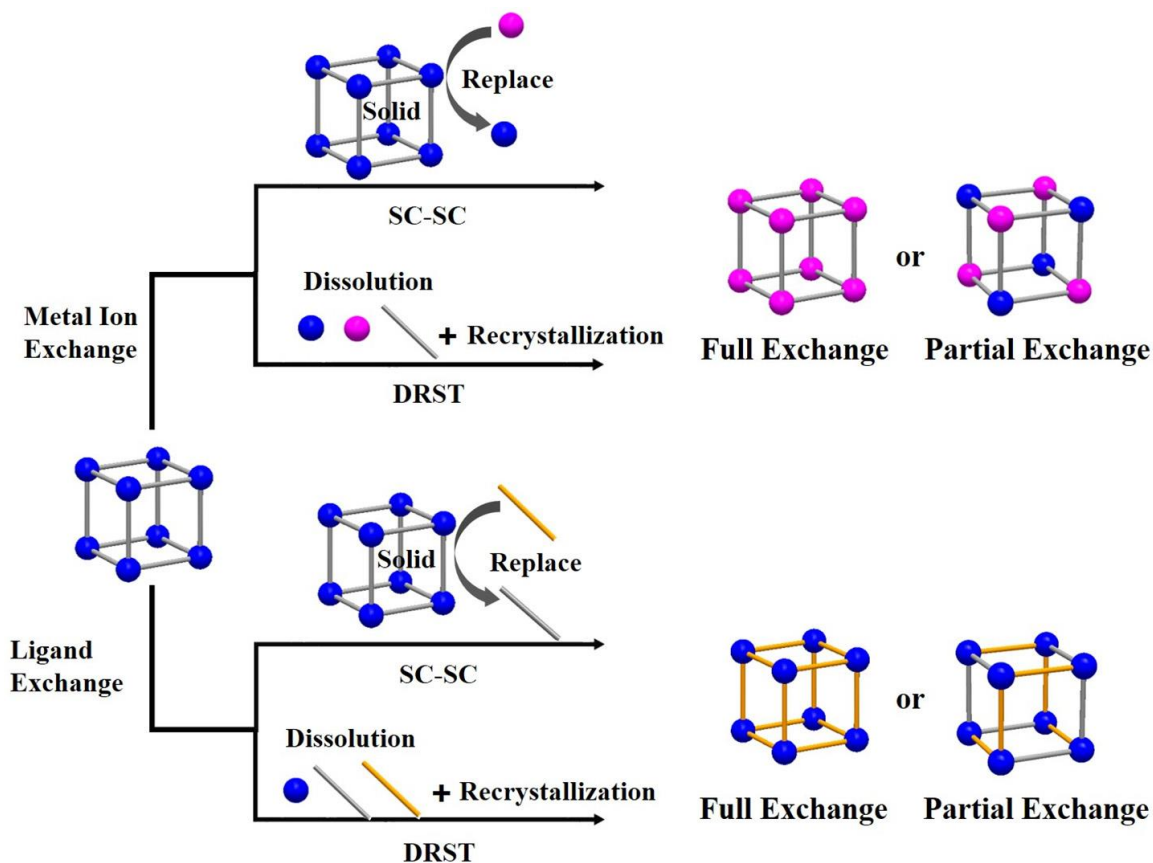

Figure 4.1 Scheme of metal ion and ligand exchange for MOFs[3]

4.3 Microwave-assisted linker exchange

Linker exchange of UiO-66 and its derivatives were well established by Seth Cohen and coworkers.[1] In a typical procedure, Solid MOF was mixed with same amount of new ligand potassium salt aqueous solution. And the exchange process will take 5 days under 55-85 °C. After the exchange reaction, the Exchanged MOF was digested by HF in DMSO-d_6, then was analyzed by NMR to get the molar ratio of new linkers and remaining original linkers. (**Figure 4.2**) The exchange ratio can achieve 76% for the exchange between UiO-66-Br and NH$_2$-BDC after 5days under 85°C. While the exchange ratio for UiO-66-NH$_2$ and Br-BDC is 43% under the same conditions.
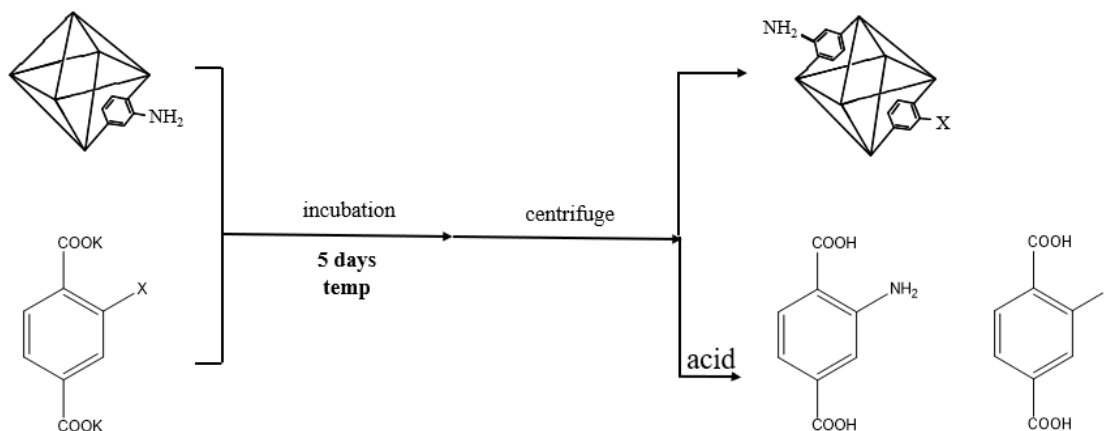
Figure 4.2 Scheme of conventional linker exchange of UiO-66-Br with NH$_2$-BDC

The reason why the regular linker exchange of UiO series takes so long time and its exchange ratio can't reach 100% is the strong Zr-Oxo interaction. Following papers in 1986[7], microwave heating has been widely utilized in the laboratory to achieve 1) reaction rate acceleration; 2) milder reaction conditions; 3) higher chemical yield;4) lower energy usage; 5) different reaction selectivity.[8-10]

Herein, we introduce microwave heating to accelerate the reaction and improve

selectivity. Reaction mixture is transferred into a microwave glass tube and sealed, then

the tube is put into a microwave reactor. The whole system is heated by microwave to

95 °C for several hours. (**Figure 4.3**)
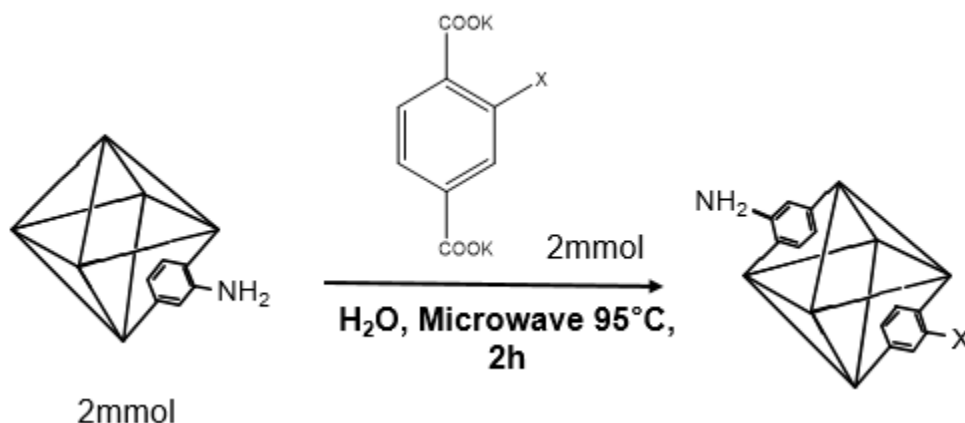
Figure 4.3 Microwave assisted linker exchange of Pd@UiO-66-NH$_2$

BDC and two functionalized BDC are choose to do microwave assisted linker exchange.

Reaction time and exchange ratio are shown in table 3. Surprisingly, the exchange ratio

for 4F-BDC linker reaches 98% which is much higher than conventional heating

result[1]. For Br-BDC and BDC linker, the exchange ratio is 49% (which is already

higher than conventional heating) and 23%. For the later one, the exchange ratio jumps to

54% when the reaction time extends to 3 hours. These results demonstrate that

microwave assisted linker exchange can achieve the similar or even higher exchange ratio

as the conventional heating in a much shorter time.
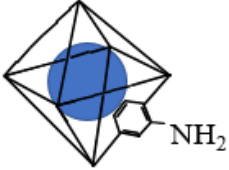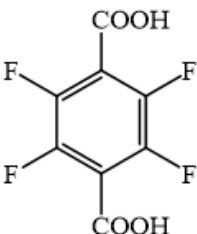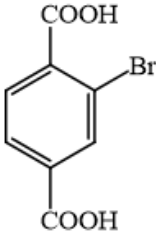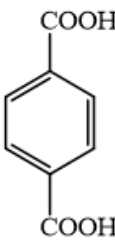
Original MOF	New Linker	Reaction conditions	Exchange ratio(%)
Pt@UiO-66-NH₂	COOH, F, F, F, F, COOH	95 °C microwave For 2h	98%
	COOH, Br, COOH		49%
	COOH, COOH		23%
		95 °C microwave For 3h	54%
Pt(PVP)@UiO-66-NH₂	4F-BDC	95 °C microwave For 2h	81%

Table 4 Microwave-assisted Linker exchange ratio

4.4 Catalytic Performance of Exchanged Pt@MOFs
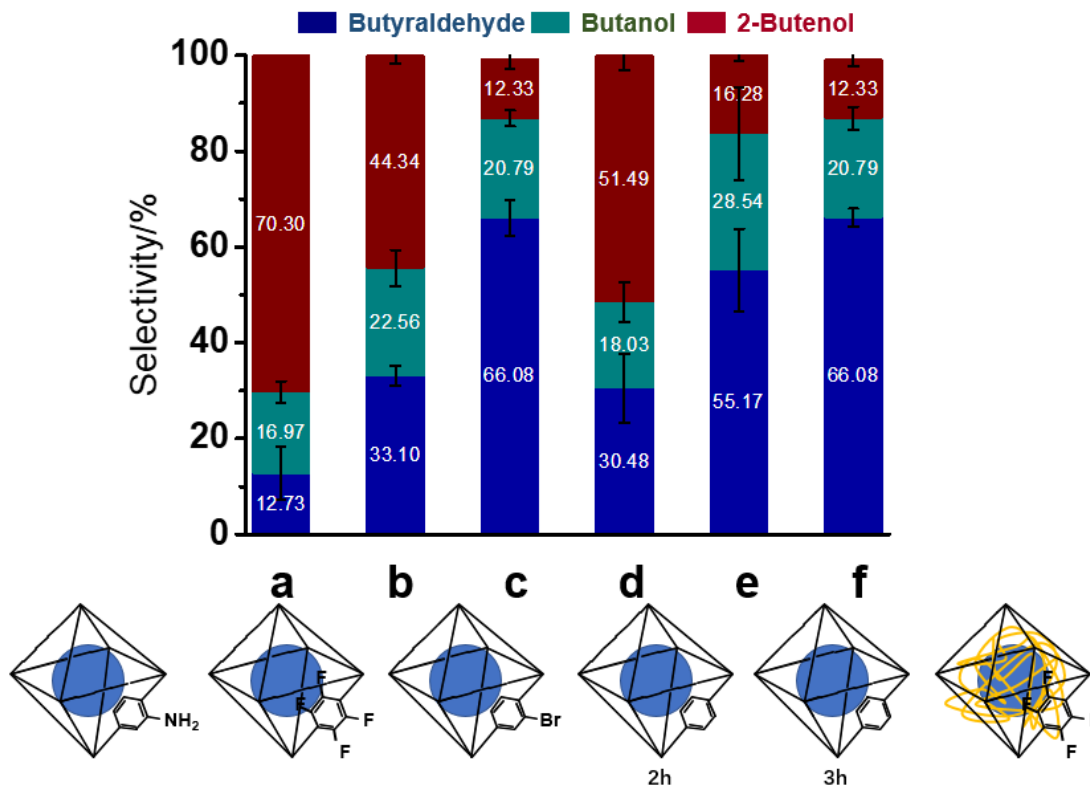
Figure 4.4 Catalytic performance of linker exchange ones, Pt@UiO-66-NH$_2$ exchanged with (a) NH$_2$-BDC (the same linker); (b) 4F-BDC (98% changed); (c)Br-BDC (49%) ;(d) BDC (2hrs 23%); (e) BDC (3hrs 54%); Pt (PVP)@UiO-66-NH$_2$ exchange with (f) 4F-BDC (81%).

After microwave assisted linker exchange, we run the same catalytic reaction in chapter 3 to see the influence of the side chain group on BDC to the catalytic performance **(Figure4.4)**. For the one exchanged with its original linker, NH$_2$-BDC, there is no significant difference in catalytic performance comparing to the intrinsic one (**Figure 3.4**), which demonstrates that the microwave heating process itself won't influence catalytic performance of our catalysts.

For the 4F-BDC linker which almost replace all the original NH_2-BDC linkers, the percentage of our target product, 2-Butenol, drops from 70% to 44.34% after exchanging. For the ones exchanged with Br-BDC and BDC, selectivity of 2-Butenol decreases even more. This general trend may indicate that either the electronic or steric effect of the amino group do have some positive influence in catalytic properties. The dramatic decrease of selectivity from 51.49% to 16.28% when exchange ratio increases from 23% to 54% for BDC exchanged ones also provide a strong support to this.

Secondly, we do the same linker exchange for the Pt (PVP)@UiO-66-NH_2, the exchange ratio is a little bit lower but still achieve 81%. Not surprisingly the reaction result suggests that there is no significant decrease in selectivity which matches with our hypothesis that steric effect do not work for Pt (PVP) since active sites of nanoparticles have already been blocked by long chain PVP.

4.5 Conclusion

In this chapter, microwave-assisted linker exchange was utilized to alter the amine group in the BDC-NH_2 linker of our Pt@UiO-66-NH_2 catalyst to explore influence of the side chain functional group to the catalytic performance. For several chosen linkers, relative high exchange ratio was achieved in a much shorter reaction time comparing to traditional heating process. Then these after-exchanged samples were tested by the same reaction as the intrinsic NP@MOF composite. For all selected linkers (BDC, 4F-BDC and 2-Br-BDC), the after-exchanged catalysts showed a decrease of selectivity of our desired product-unsaturated alcohol. Based on these results, comparing to other functional group, the

existence of amine group does have a positive effect on the activity and selectivity of this reaction, which may be caused by the electronic density increase in Pt atom due to the Pt-N interaction.

However, it is still not clear that how the functional group on BDC linkers influence the catalytic performance. Briefly speaking, the functional groups have both electronic and steric effects to the active sites. Taft equation (**Figure 4.5**) which was developed by Robert W. Taft in 1952[11-13] is a linear free energy relationship (LFER) used to the study of reaction mechanisms in physical organic chemistry and build quantitative structure–activity relationships for organic compounds. By measuring the reaction rate constant of different functionalized linker exchanged catalyst and comparing to the rate constant of reference group, the sensitivity factors of electronic and steric effect can be solved and we can analyze the influence of function group to the active sites quantitatively.

$$\log\left(\frac{k_s}{k_{CH_3}}\right) = \rho^*\sigma^* + \delta E_s$$

Taft equation

σ^* polar substituent constant
E_s steric substituent constant
ρ^* sensitivity factor of σ^*
δ sensitivity factor of E_s

Figure 4.5 Taft equation

In order to perform quantitative structure–activity study using Taft equation, we have to prepare entirely exchanged Pt@UiO-66-NH$_2$ with functionalized linkers. Our microwave-assisted linker exchange approach already shows better performance than the traditional

heating method. However, we still need to optimize reaction conditions to achieve 100%

exchange ratio for more linkers.

4.6 Methods

General Considerations. Unless otherwise stated, all the reactions were carried out in the

air without taking any precaution to protect reactions from oxygen or moisture. N, N-

Dimethylformamide (Sigma-Aldrich, 99.8%), Potassium hydroxide (KOH, Sigma-

Aldrich, ≥85%), tetrafluoroterephthalic acid (4F-BDC, Sigma-Aldrich, 97%), terephthalic

acid (BDC, Sigma-Aldrich, 98%), 2-bromoterephthalic acid (Br-BDC, Sigma-Aldrich,

95%), hydrochloric acid (HCl, Sigma-Aldrich, 37%), crotonaldehyde (Sigma-

Aldrich, >99%) were purchased from the indicated sources and used without further

purification. Hydrogen (Airgas, 99.999%) and Nitrogen (Airgas, 99.999%) were used for

heterogeneous catalysis.

^{1}H and ^{19}F Nuclear magnetic resonance (NMR) spectroscopy was performed on Varian

500 MHz and 600 MHz NMR spectrometers. Samples were prepared by digesting

approximately 10 mg of UiO-66-NH$_2$ or linker-exchanged UiO-66-NH$_2$ samples with

sonication in 580 μL of DMSO-d$_6$ and 20 μL of HF (48% aqueous solution). For ^{19}F-

NMR, 10 μL of F-CH$_2$COOH was added as an internal standard. All of the NMR

measurements were performed with 90- degree pulse and a recycle delay larger than 5

times of spin-lattice relaxation time between each transient to ensure complete relaxation

of the observed spins.

Microwave assisted post synthetic linker exchange between UiO-66-NH₂ and 4F-BDC: Tetrafluoroterephthalic acid (57.6 mg, 0.2mmol) was dissolved in 4% KOH aqueous solution(2mL). 1M HCl aqueous solution was added drop by drop to neutralize the solution to pH=7. This solution and Pt@UiO-66-NH₂ (57mg, 0.2mmol equiv. of benzene ring) were added to a 5mL microwave tube with a small magnetic stirring bar, then sealed with a cap. The sealed tube was put into a microwave reactor and microwaved to 95 ℃ for 2 hours with stirring. When the mixture cooled down to room temperature, the cap was removed by cap opener and the mixture was moved to a centrifuge tube. The mixture was centrifuged and the aqueous phase decanted. Then precipitant was washed with 10mL menthol for 3 times, and then vacuum dried overnight. Linker exchange of other ligands and MOFs mentioned in this chapter are performed by simply change the chemicals or reaction time in this procedure.

Liquid Phase hydrogenation of crotonaldehyde: In a typical procedure, a certain amount of catalyst was dispersed in 2.4 mL isopropanol solution, and 100 μL trans-crotonaldehyde (1.19 mmol, Aldrich >99%) were added into the above solution. Subsequently, the solution was transferred into a 4.0-mL ampule using a 9" glass pipet. These ampules were arranged in a 500 mL stainless steel Parr reactor that contained a thermocouple to ensure thermostatic reactions. The reactor was placed on the top of a Ika RCT-basic hot plate. The reactor vessel was purged with H₂ for 3 times, and the final H₂ pressure of the vessel was set at 3.0 MPa. During the catalytic process, the reaction solution was magnetically stirred with the speed of 800 rpm at desired temperature for the 18 hours. After that, the catalysts were separated by centrifugation, and the obtained

reaction solution was analyzed by gas chromatography-mass spectrometry (GC-MS, Shimadzu, GC-MS-QP2010 Ultra, column: SH-Rtx-Wax, 60 m × 0.25 mm × 0.5μm)

4.7 Reference

1.   Kim, M., et al., *Postsynthetic ligand exchange as a route to functionalization of 'inert' metal–organic frameworks.* Chem. Sci., 2012. **3**(1): p. 126-130.

2.   Karagiaridi, O., et al., *Solvent-assisted linker exchange: an alternative to the de novo synthesis of unattainable metal-organic frameworks.* Angew Chem Int Ed Engl, 2014. **53**(18): p. 4530-40.

3.   Xu, M.-M., et al., *Exchange reactions in metal-organic frameworks: New advances.* Coordination Chemistry Reviews, 2020. **421**.

4.   Marshall, R.J. and R.S. Forgan, *Postsynthetic Modification of Zirconium Metal-Organic Frameworks.* European Journal of Inorganic Chemistry, 2016. **2016**(27): p. 4310-4331.

5.   Islamoglu, T., et al., *Postsynthetic Tuning of Metal–Organic Frameworks for Targeted Applications.* Accounts of Chemical Research, 2017. **50**(4): p. 805-813.

6.   Yin, Z., et al., *Recent advances in post-synthetic modification of metal–organic frameworks: New types and tandem reactions.* Coordination Chemistry Reviews, 2019. **378**: p. 500-512.

7.   Gedye, R., et al., *The use of microwave ovens for rapid organic synthesis.* Tetrahedron Letters, 1986. **27**(3): p. 279-282.

8.   Polshettiwar, V. and R.S. Varma, *Microwave-Assisted Organic Synthesis and Transformations using Benign Reaction Media.* Accounts of Chemical Research, 2008. **41**(5): p. 629-639.

9.   Chen, T., et al., *Fast synthesis of carbon microspheres via a microwave-assisted reaction for sodium ion batteries.* Journal of Materials Chemistry A, 2014. **2**(5): p. 1263-1267.

10.   Lv, T., et al., *Enhanced photocatalytic degradation of methylene blue by ZnO-reduced graphene oxide composite synthesized via microwave-assisted reaction.* Journal of Alloys and Compounds, 2011. **509**(41): p. 10086-10091.

11.   Taft, R.W., *Linear Free Energy Relationships from Rates of Esterification and Hydrolysis of Aliphatic and Ortho-substituted Benzoate Esters.* Journal of the American Chemical Society, 1952. **74**(11): p. 2729-2732.

12.   Taft, R.W., *Polar and Steric Substituent Constants for Aliphatic and o-Benzoate Groups from Rates of Esterification and Hydrolysis of Esters1.* Journal of the American Chemical Society, 1952. **74**(12): p. 3120-3128.

13.   Taft, R.W., *The Separation of Relative Free Energies of Activation to Three Basic Contributing Factors and the Relationship of These to Structure.* Journal of the American Chemical Society, 1953. **75**(18): p. 4534-4537.

Chapter 5 Future Directions

A series of metal nanoparticles@MOFs are synthesized via one-pot *in situ* method which take advantages of two traditional strategies and avoid their biggest issues. The amine group in the organic linker of UiO-66-NH$_2$ take the place of capping agent PVP in the formation of metal nanoparticles which avoids the active sites of encapsulated metal nanoparticles being blocked by PVP. We tested its catalytic performance with the selective hydrogenation of a α, β-unsaturated aldehyde, crotonaldehyde, and our catalyst has much higher activity than the one with PVP. Additionally, we believe the uniform pores of UiO-66-NH$_2$ could provide a steric effect to improve the selectivity of this reaction to our desired product, unsaturated aldehyde. And experiment results support this hypothesis, our catalyst can achieve 70% selectivity to 2-Butenol (our target product), which is higher than not only merchant Pt catalyst but also physical mixture of Pt nanoparticles and MOF. Furthermore, the amine group on the linker plays an important role in the synthesis process, but how will the side chain functional group influence the catalytic performance of our catalysts? Thus, we perform the linker exchange to replace the NH$_2$-BDC linker with BDC and functionalized linkers and the replaced ones show a significant decay in selectivity of 2-Butenol which means the existence of amine group is essential to the catalytic performance of our catalysts.

In this thesis, we demonstrate a synthetic mythology which is promising to adjust catalytic performance metal nanoparticles. A step further, we chose the selective hydrogenation of crotonaldehyde as model reaction to demonstrate the well-defined direct contact metal nanoparticles and MOF interface and spatial confinement of MOF

pores could increase the selectivity. However, the highest selectivity towards our desired product we achieved is still not as high as the state of art reported results of selective hydrogenation of other α, β-unsaturated aldehydes[1-3], which means there are still lots of works to do to optimize this system. One possible method is to replace the side chain function group to tune the electronic and steric environment of the metal-MOF interface, this requires deeper understanding of the impacts we are planning to do a systematic scanning of BDC derivatives and use Taft equation to analysis the electronic and steric effects of different side chain functional groups. As Pt/Pd are widely used as catalysts, the spatial confinement and clean surface of encapsulated nanoparticles should allow our catalyst to be utilized for other reactions, like selective oxidation of diols. [4] Also, some other MOFs like MIL-101[1, 5]which has a much larger pore size of 1.6nm can also be used to replace UiO-66-NH$_2$, which could be utilized to achieve selectivity for other substrates and reactions. For the one-pot synthesis approach, by choosing proper metal percussors and organic linkers, this facile synthesis method should be expanded to other metal nanoparticles@MOFs structures. We believe our research could provide a choice to people who want to tune the catalytic performance of heterogenous catalysts.

5.1 Reference

1. Zhao, M., et al., *Metal–organic frameworks as selectivity regulators for hydrogenation reactions.* Nature, 2016. **539**(7627): p. 76-80.

2. Stephenson, C.J., et al., *Chemoselective Hydrogenation of Crotonaldehyde Catalyzed by an Au@ZIF-8 Composite.* ChemCatChem, 2016. **8**(4): p. 855-860.

3. Lan, X., et al., *Geometric effect in the highly selective hydrogenation of 3-methylcrotonaldehyde over Pt@ZIF-8 core–shell catalysts.* Catalysis Science & Technology, 2017. **7**(12): p. 2601-2608.

4.   Zhang, W., et al., *Site-Selective Catalysis of a Multifunctional Linear Molecule: The Steric Hindrance of Metal-Organic Framework Channels.* Advanced Materials, 2018. **30**(23).

5.   Bhattacharjee, S., C. Chen, and W.-S. Ahn, *Chromium terephthalate metal–organic framework MIL-101: synthesis, functionalization, and applications for adsorption and catalysis.* RSC Advances, 2014. **4**(94): p. 52500-52525.